Applied and Computational Mechanics 20 (2026) 41–66

Numerical investigation of fluid flow in a T-shaped lid-driven cavity by CFD

D. S. Ravichandran[a], D. A. Perumal[b,*], R. Manimaran[c]

[a] *Department of Production Engineering, National Institute of Technology Agartala, Barjala, Jirania, Tripura 799046, India*
[b] *Department of Mechanical Engineering, National Institute of Technology Karnataka, Surathkal, Mangalore 575025, India*
[c] *School of Mechanical Engineering, Vellore Institute of Technology Chennai, Chennai, Tamil Nadu 600127, India*

Received 18 August 2025; accepted 13 February 2026

Abstract

The present research aims at providing a numerical fluid flow prediction of the less explored T-shaped lid-driven cavity problem. It is solved two ways, first using a finite-difference-method-based vorticity-stream function formulation that is applied to the two-dimensional incompressible Navier-Stokes equations and then by using the SIMPLE algorithm implemented in the finite-volume-method-based OpenFOAM system. Firstly, a numerical in-house code is developed for a classical lid-driven square cavity problem, and successively verified by comparing it with results from the literature. Once the code's credibility is established, the fluid flow characteristics are thoroughly investigated considering three different wall motions: single-sided, double-sided with co-directional wall motion, and double-sided with counter-directional motion. The investigation also focuses on how the fluid flow characteristics are influenced by both the Reynolds number of the flow and the aspect ratio of the domain. Through numerical simulations, the centerline velocity profiles are plotted, and also the structure and formation of vortices in a T-shaped cavity are compared between both finite difference and finite volume schemes. As the Reynolds number of the domain rises, many recirculation zones are formed, the fluid is shown to flow faster in the wall-driven enclosures. As the aspect ratio increases the strength of the vortices diminishes at the walls of the computational domain.
© 2026 University of West Bohemia in Pilsen.

Keywords: vorticity-stream function, SIMPLE algorithm, T-shaped cavity, Reynolds number

1. Introduction

The most primitive form of the lid-driven cavity problem consists of a moving top wall and other stationary bounding walls [24]. In the field of fluid mechanics, this makes an interesting case to study, especially due to the internal re-circulating flows that are created when the driving lid pushes the fluids that are bound by walls. Recently, thorough investigations have been conducted on the flow generated by two walls moving both in co-directional and counter-directional directions [12, 13]. Later, there has been a growing interest to explore different complex cavity shapes, such as triangular and trapezoidal L-shaped cavities, in the lid-driven cavity problem [1, 6, 10, 20, 27].

Researchers have also been able to observe the varying trends in flow patterns due to the changes in cavity aspect ratio. In this case, it is worthy to note that the effect of a particular aspect ratio is different for different Reynolds numbers. Initial research of the two-dimensional steady flow in a single lid-driven cavity was carried out by Burgraff [5] for a square cavity, while Pan and Acrivos [17] investigated a variety of geometrical aspect ratios for the same problem.

*Corresponding author. Tel.: +91 915 986 05 35, e-mail: perumal@nitk.edu.in.
https://doi.org/10.24132/acm.2026.1029

The need for benchmark solutions for code developers led Ghia et al. [8] to study lid-driven cavities for high Reynolds number flows using a vorticity-stream function formulation and to establish exemplary results. Shen [25] and Goodrich et al. [9] worked on a variant of the single sided two-dimensional lid driven cavity that had time dependent results. In [13], Kuhlmann et al. expanded the investigation into the double-sided moving wall configuration with counter-directional motion. They performed numerical investigations of the two-dimensional lid-driven cavities and conducted experiments for the three-dimensional problem for various aspect ratios and Reynolds numbers. In their study, they concluded that the double-sided configuration of the lid-driven cavity was ideal for capturing the characteristics of viscous corner eddies. Perumal and Dass [22] also investigated a double-sided lid driven cavity problem with both co-directional and counter-directional wall motions using an alternate direction implicit technique implemented through the finite difference method. In [15], Moffatt discovered that the interaction between the wall jet and the pressure gradient that is induced by the corner of the cavity leads to a separation of the jet from the wall and the formation of an additional swirling flow pattern in the corner of the cavity domain. These corner eddies were termed as Moffatt vortices. A detailed description of these eddies is also given by Kelmanson and Lonsdale in [11].

Many geometrical shapes have been studied throughout time as far as the lid-driven cavity problem is concerned. In [14], McQuain et al. studied the effect of geometry on the flow structure. The geometry was changed from a rectangle to a triangle through a series of trapezoids and the authors concluded that a triangular cavity would be less effective for studying heat and mass transfer due to a large stagnant region at the center. Bhopalam et al. [2, 3] investigated a cross-shaped cavity and an L-shaped cavity separately and thoroughly examined the extent of fluid mixing in these geometries. The classical lid-driven square cavity is extended by deep cavity flow in [19]. The authors studied different Reynolds numbers and aspect ratios of the deep cavity domain. The numerical study of lid driven cavity is extended by a corrugated bottom, obstacles and wave length inside the computational domain [4, 18, 21, 23, 26]. Researchers studied fluid flow and heat transfer characteristics in terms of the Reynolds number and aspect ratio of the domain. In [4], Bisht et al. investigated lid-driven cavity flow with a corrugated bottom wall and demonstrated that surface corrugation significantly alters vortex structures and enhances mixing, highlighting the strong influence of geometric modifications on confined flows. Rajan and Perumal [23] analyzed lid-driven cavities with internal obstacles of various shapes using the lattice Boltzmann method (LBM), showing that an obstacle geometry strongly affects flow separation and recirculation patterns. In [21], Perumal and Dass validated the applicability and accuracy of the LBM for incompressible viscous flows, providing a numerical foundation for later cavity-flow studies using this method. Shetty et al. [26] studied cavity flows in bounded domains with non-standard cavity shapes and demonstrated the sensitivity of vortex dynamics to cavity geometry, reinforcing the need to study complex cavity configurations. In [18], Park performed direct numerical simulations of lid-driven cavities over a wide range of the Reynolds number, offering high-fidelity benchmark data for the verification of numerical schemes.

On the basis of literature review and to the best knowledge of the authors, the T-shaped lid-driven cavity has received much less attention from researchers in comparison to other complex shapes. Given its practical applications, the present T-shaped cavity deserves a thorough investigation as the flow within it is an idealized representation of several engineering situations, such as the flow over cutouts, designs and repeated slots on the walls of heat exchangers in electronic cooling devices. Since T-shaped cavities are extensively used as heat exchangers in electronic cooling devices, this study helps us to identify the efficiency of fluid mixing that is facilitated inside such cavities. This paper delves into the behavior of a T-shaped cavity and

investigates the effects of wall motions, Reynolds number, and aspect ratios on the incompressible flow inside the cavity. The numerical method used for solving the fluid flow involves a vorticity-stream function formulation that is implemented with the help of a finite difference scheme. A variety of streamline patterns are presented along with centerline velocity plots that would help us make logical inferences with regards to the mixing effects. Additionally, the nature of secondary, tertiary and corner vortices for different aspect ratios and Reynolds numbers are analyzed.

The current study presents a numerical prediction of the flow induced inside a T-shaped lid-driven cavity with three distinct wall motions: single-sided, double-sided with co-directional motion, and double-sided with counter-directional motion. The paper is structured into four main sections as follows: Section 2 outlines the problem statement and defines the computational domain where simulations will be conducted using an in-house code and OpenFOAM. In Section 3, the numerical scheme employed in the study is described, and the code's correctness is established through verification tests. Once the code's reliability is confirmed, Section 4 showcases the results and discussions derived from the simulated scenarios. Finally, Section 5 delivers a comprehensive summary that concludes the entire study.

2. Numerical method

2.1. Problem formulation

In this study, our specific aim revolves around the examination of flow attributes within the T-shaped geometry of a lid-driven cavity, Fig. 1. It is important to mathematically define parameters such as the Reynolds number (Re) and the aspect ratio (AR) for all the configurations, as their effects are particularly investigated in this study. Consistently throughout the investigation, a constant velocity magnitude U is applied on the lids of the cavity. The two characteristic lengths of the cavity are given by H and l and the kinematic viscosity of the fluid is given by ν.

The mathematical definitions of the parameters used in the study are written as follows:

$$\mathrm{Re} = \frac{UH}{\nu}, \qquad \mathrm{AR} = \frac{H-2l}{H}. \tag{1}$$

Further, the empirical expression

$$h_1 = 2l \tag{2}$$

relating the two dimensions h_1 and l, as shown in Fig. 1, is maintained for all simulations to preserve the thickness of the cavity along the top column.

2.2. Solver based on the vorticity-stream function formulation

The current study implements a finite difference code that solves the two-dimensional (2D) Navier-Stokes equations that are represented in the form of finite-difference-based vorticity and stream function. The equations are as follows:

$$\frac{\partial^2\psi}{\partial x^2} + \frac{\partial^2\psi}{\partial y^2} = -\omega, \tag{3}$$

$$\frac{\partial\omega}{\partial t} + u\frac{\partial\omega}{\partial x} + v\frac{\partial\omega}{\partial y} = \frac{1}{\mathrm{Re}}\left(\frac{\partial^2\omega}{\partial x^2} + \frac{\partial^2\omega}{\partial y^2}\right), \tag{4}$$

where ω is the amount of rotation in terms of vorticity, ψ is the stream function, Re is the Reynolds number, and u and v are the velocity components in the x- and y-directions, respectively. We achieve the steady state solution by coupling the discretized form of the governing

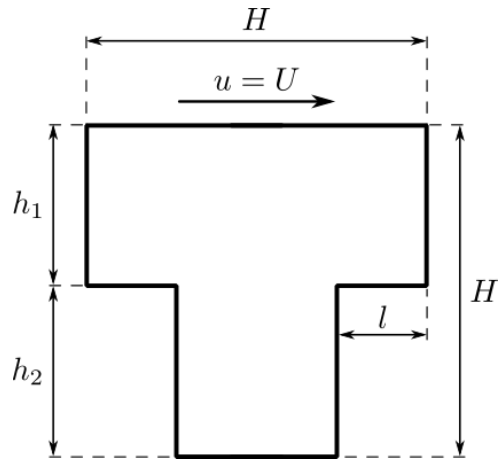

Fig. 1. Schematic diagram of the T-shaped lid-driven cavity

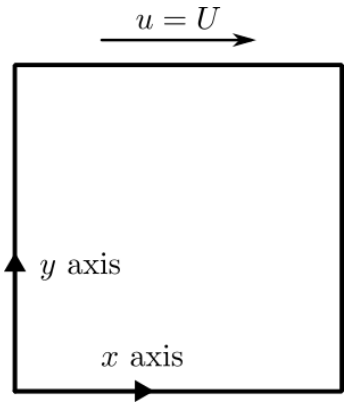

Fig. 2. Conventional lid-driven cavity configuration with boundary conditions

momentum equation in terms of stream function-vorticity formulation, and further by solving it sequentially in time using an iterative procedure. However, using an explicit scheme with a forward time-marching approach of first order accuracy with derivative term and a central spatial discretization often leads to a very small time step due to stability limitations. Consequently, the convergence to the steady state for higher Reynolds numbers becomes extremely slow. Thus, equipping a central space-differencing poses significant challenges in achieving the final result. With respect to this issue, a first-order accurate forward-differencing method is utilized for the flow distribution terms. At the moving walls, a velocity of $U = 1$ is applied and, at the stationary walls, a velocity value of $u = 0$ is applied. It is very important to note that even though this modification reduces the computational time, it could potentially compromise the accuracy of the solutions by a slight margin.

2.3. SimpleFoam solver

SimpleFoam is a steady-state solver for turbulent, incompressible flows that uses the semi-implicit method for pressure linked equations (SIMPLE algorithm). The solver employs an approach of segregated solutions for the continuity and Navier-Stokes equations

$$\nabla \cdot \boldsymbol{v} = 0, \tag{5}$$

$$\varrho \left[\frac{\partial \boldsymbol{v}}{\partial t} + (\boldsymbol{v} \cdot \nabla) \boldsymbol{v} \right] = -\nabla p + \nabla \cdot \boldsymbol{\tau} + \varrho \boldsymbol{g}, \tag{6}$$

where ϱ is the density of the fluid, $\boldsymbol{v} = [u, v]^T$ indicates the velocity vector, p is the pressure, $\boldsymbol{\tau}$ is the stress tensor, and $\boldsymbol{g}$ denotes the vector of gravitational acceleration. This implies that the velocity and pressure variables that made up the system's equations are solved one after the other, with the updated variables from the earlier equations being incorporated into the latter one. The non-linearity in the momentum equations can be fixed by computing it using the pressure and velocity values from the previous iteration. In order to prevent the momentum and pressure equations from decoupling and to avoid the subsequent emergence of high frequency oscillations in the numerical solution, a pressure dependency is included. The pressure equation is created using the momentum and continuity equations. Until convergence, the aforementioned iterative solution process is repeated.

Table 1. Grid independence study for $\mathrm{Re} = 1\,000$

Method	Grid size	$u_{\min}\,[-]$	$v_{\min}\,[-]$
Vorticity-stream function method	101×101	$-0.374\,63$	$-0.499\,67$
	129×129	$-0.380\,72$	$-0.509\,52$
	161×161	$-0.382\,81$	$-0.515\,47$
OpenFOAM	10^5	$-0.381\,54$	$-0.498\,54$
	$3 \cdot 10^5$	$-0.382\,61$	$-0.514\,78$
	$5 \cdot 10^5$	$-0.382\,83$	$-0.514\,95$

2.4. Grid independence study

To ensure the accuracy of our code while investigating the flow inside the T-shaped cavity, it is important to carry out a grid independence study. In the present study, two different approaches, namely the vorticity-stream function method and OpenFOAM, are used. To ensure grid-independent results, an analysis was performed for $\mathrm{Re} = 1\,000$ with results listed in Table 1. Three different grids, namely coarse (101×101), medium (129×129), and fine (161×161), are used in the in-house code based on the vorticity-stream function formulation. From Table 1, it is apparent that the percentage deviation of coarse grid from the fine grid is minimal (within 2 %) in predicting velocity values. In the present study, the fine grid (161×161) is used for in-house code simulations. In the case of OpenFOAM simulations, a coarse (10^5 cells), a medium ($3 \cdot 10^5$ cells), and a fine ($5 \cdot 10^5$ cells) grid are used to predict u-velocity values. From Table 1, one can notice that the percentage error is minimal and it is insignificant when using coarse or fine grid in the OpenFOAM simulation.

2.5. Code verification study

For further verification of our code, it is crucial to compare its results with existing data from the literature. A comparative study was done between the results from the finite-difference-based vorticity-stream function code and the calculations done by the multigrid-based method [8] for a single lid-driven square cavity (Fig. 2) at a Reynolds number of 100. Referring to the schematic drawing in Fig. 2, the top wall is moving with a constant velocity $(u = U)$, whereas the other three walls are taken as stationary $(u = 0)$. Due to the movement of the top wall momentum is diffused inside the cavity domain. For the purpose of code verification, centerline velocity profiles are compared at different Reynolds numbers, Fig. 3. In this case, a very fine grid is used. The convergence criterion of 10^{-5} is set for velocity components. It is apparent that the in-house code and the multigrid codes are in good agreement. To understand the agreement between the finite difference method (FDM) in-house code and the finite volume method (FVM) OpenFOAM code, the position of vortices at $\mathrm{Re} = 100$ are listed in Table 2.

Table 2. Location of vortex cores in the single-sided lid-driven square cavity at $\mathrm{Re} = 100$

Study	Primary vortex (x, y)	Bottom left (x, y)	Bottom right (x, y)
In-house code	(0.5316, 0.5662)	(0.0830, 0.0771)	(0.8640, 0.1124)
Ghia et al. [8]	(0.5313, 0.5625)	(0.0859, 0.0781)	(0.8594, 0.1094)
OpenFOAM	(0.5215, 0.5672)	(0.0825, 0.0743)	(0.8623, 0.1217)

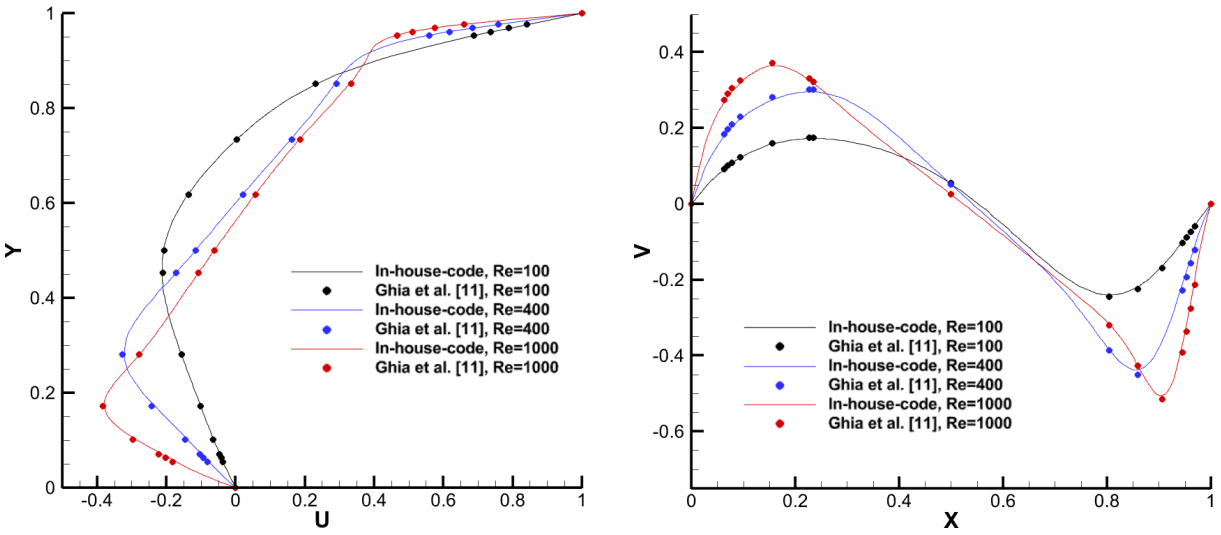

(a) u-velocity profile (b) v-velocity profile

Fig. 3. Velocity profiles along the centerline for a single-sided lid-driven square cavity at different Reynolds numbers

Excellent agreement was achieved between our in-house code, OpenFOAM (using SimpleFoam) and the data from the literature, indicating that our code accurately captures the flow characteristics. It can be noted that the existing numerical results of the multigrid-based solver by Ghia et al. [8], the present in-house code and OpenFOAM are capturing vortex positions accurately. It is observed that a slight variation between the FDM-based in-house code and the FVM-based OpenFOAM code occurs. The reason for this is that the FDM-based approach is first-order accurate, whereas the FVM-based approach is second-order accurate. This comparison serves as an important foundation for our research problem. The error calculated between in-house code and OpenFOAM is found to be less than 5 % and hence both the codes are considered for further study.

Next, to ensure a good prediction of flow also inside the T-shaped cavity, we compare the code results with available experimental and CFD results by Naeem [16]. Table 3 shows the comparison of the measured PIV data with numerical data from the in-house code and OpenFOAM. It is apparent that there is a deviation due to numerical diffusion and modeling assumptions. The OpenFOAM results at $\mathrm{Re} = 1\,250$ are comparable with PIV results from [16] and found to be within 10 % except at locations $y = 4$ mm, $y = 6$ mm, and $y = 8$ mm, where the shear layer or the gradient of the x-component of velocity is not resolved along with the same phenomenon as observed in [16]. The reason for the significant deviation may come from the inaccuracy in laser sheet alignment at precise locations within millimeter accuracies.

3. Results and discussion

In this study, the fluid flow inside the T-shaped cavity was investigated for three different types of moving wall configurations, namely single-sided and double-sided with both co-directional and counter-directional motions. Various aspect ratios ($\mathrm{AR} = 0.2$, 0.5, and 0.8) along with different Reynolds numbers ($\mathrm{Re} = 200$, 500, and $1\,000$) are considered. With its unique physical features, the T-shaped cavity is expected to yield intriguing results, particularly due to its protrusions at the top and bottom, which differentiate it from a square cavity. It is anticipated

Table 3. Comparison of U-velocities measured by the PIV method [16] and computed by CFD [16], in-house code and OpenFOAM (Y denotes the axis along the vertical direction of the cavity)

Y	PIV [16]	CFD [16]	in-house code	OpenFOAM
0	–	0.042 30	0.042	–
1	0.026 60	0.022 13	0.021	0.025 41
2	0.028 59	0.019 75	0.019	0.027 38
4	0.027 77	0.015 44	0.015	0.016 73
6	0.021 11	0.010 82	0.011	0.010 17
8	0.004 36	0.006 41	0.007	0.006 48
10	−0.010 24	0.002 08	0.002	−0.010 09
12	−0.019 80	−0.001 55	−0.002	−0.018 30
14	−0.026 70	0.005 72	−0.006	−0.025 20

that there will be an increase in the number of recirculation zones for this very same physical peculiarity.

3.1. Single-sided T-shaped lid-driven cavity

By studying the results of the single wall motion, it can be noted that for AR $= 0.2$ the number of recirculation zones remains constant throughout for different Reynolds numbers, Fig. 4. It is evident that since the cavity is narrow for this particular aspect ratio, it behaves similarly to a deep cavity [19] as it forms many recirculation zones in the narrow cavity. A similar result has also been obtained for corrugated cavities and other shapes of the cavity domain [4, 7, 16, 18, 21, 23, 26]. The case of streamline patterns for AR $= 0.5$ produces interesting results to visualize the steady state configuration change for each Reynolds number, Fig. 5. For $\mathrm{Re} = 200$, only two recirculation zones are observed, whereas for $\mathrm{Re} = 500$, it is noted that an additional secondary vortex is also formed in response to the continuous shearing movement produced by the primary vortex.

At $\mathrm{Re} = 1\,000$, it is found that one of the corner eddies from the left side coalesces with the secondary vortex from the bottom half of the cavity at the steady state, Fig. 6. Streamline patterns AR $= 0.8$ does not produce many variations with one large recirculation zone and several corner eddies that are also termed as Moffatt vortices. These vortices form at sharp concave edges [15]. They are also visible at the corners for AR $= 0.5$, and they keep growing as the Reynolds number increases. However, at AR $= 0.8$, the Moffatt vortex from the left does not grow large enough to coalesce with the secondary vortex from the bottom. The reason behind this difference is attributed to the cavity's small step size and the lack of energy in the flow. In general, the in-house code and OpenFOAM results show great agreement, except for a few minor differences such as the fundamental configuration of the primary vortex at AR $= 0.2$ and the Moffatt vortices that are absent at $\mathrm{Re} = 200$ for the in-house code.

The centerline velocity profiles presented in Fig. 7 provide valuable insights into the extent of fluid mixing. From the plot, it is also evident that the magnitude of the extrema increases with the increase in Reynolds number for the u-velocity. However, it is interesting to note that for the v-velocity, the magnitude of the extrema is largest for AR $= 0.5$. This is because the concave corner of the cavity lies closer to the horizontal line that bisects the top region of the cavity. In addition to that, the v-velocity trend varies very drastically from negative to positive values.

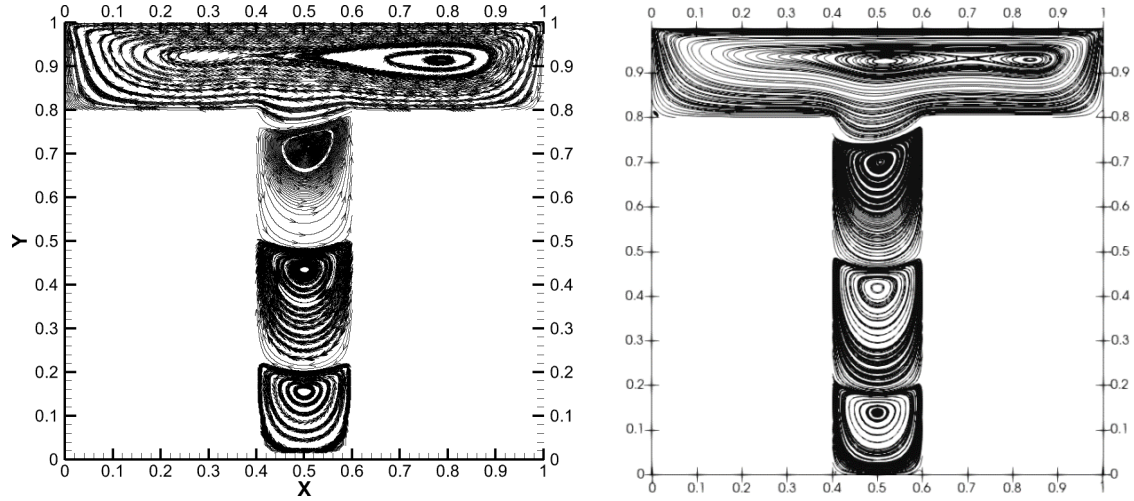

(a) Re = 200

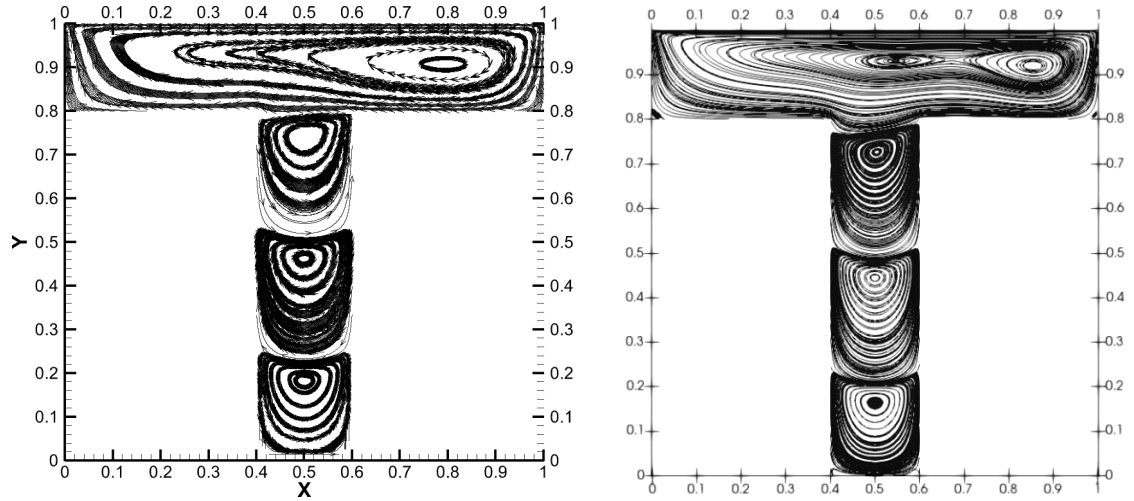

(b) Re = 500

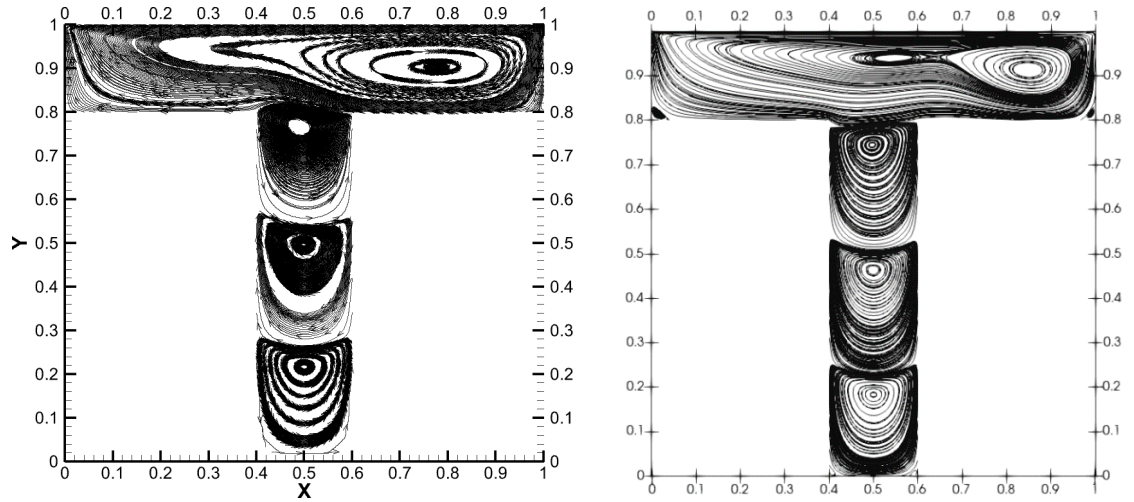

(c) Re = 1 000

Fig. 4. Streamline patterns in the single-sided T-shaped lid-driven cavity for different Reynolds numbers (AR = 0.2): (*left*) in-house code, (*right*) OpenFOAM

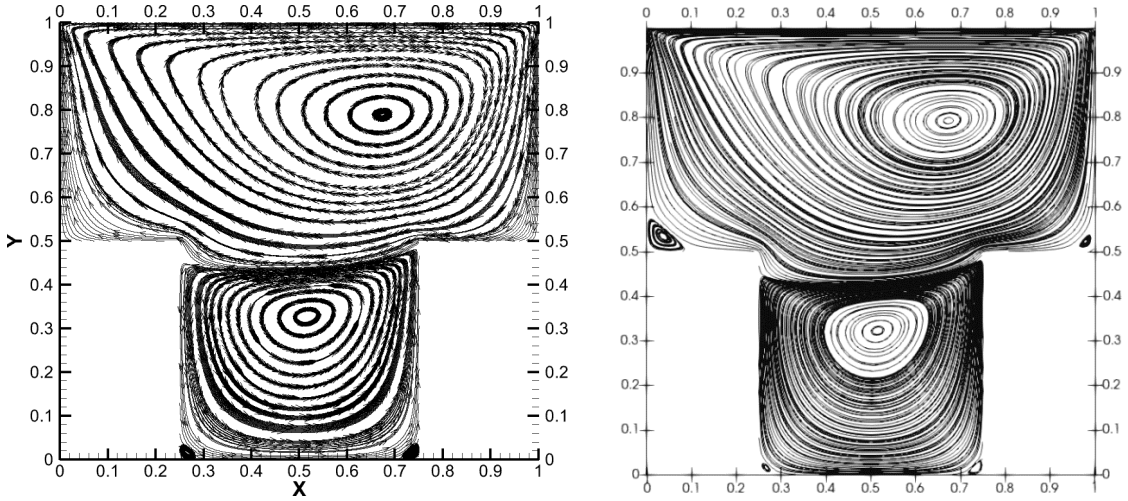

(a) $\mathrm{Re} = 200$

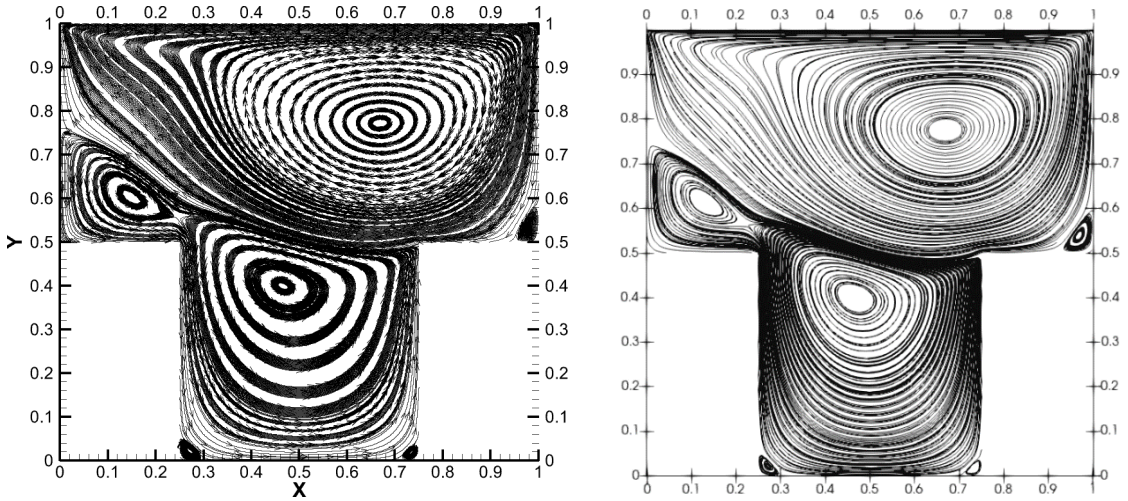

(b) $\mathrm{Re} = 500$

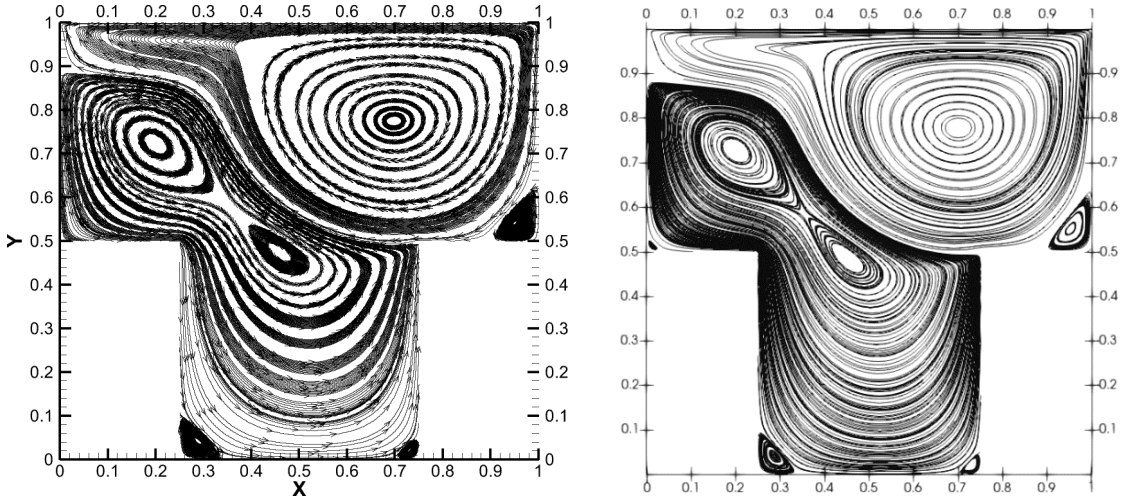

(c) $\mathrm{Re} = 1\,000$

Fig. 5. Streamline patterns in the single-sided T-shaped lid-driven cavity for different Reynolds numbers ($\mathrm{AR} = 0.5$): (*left*) in-house code, (*right*) OpenFOAM

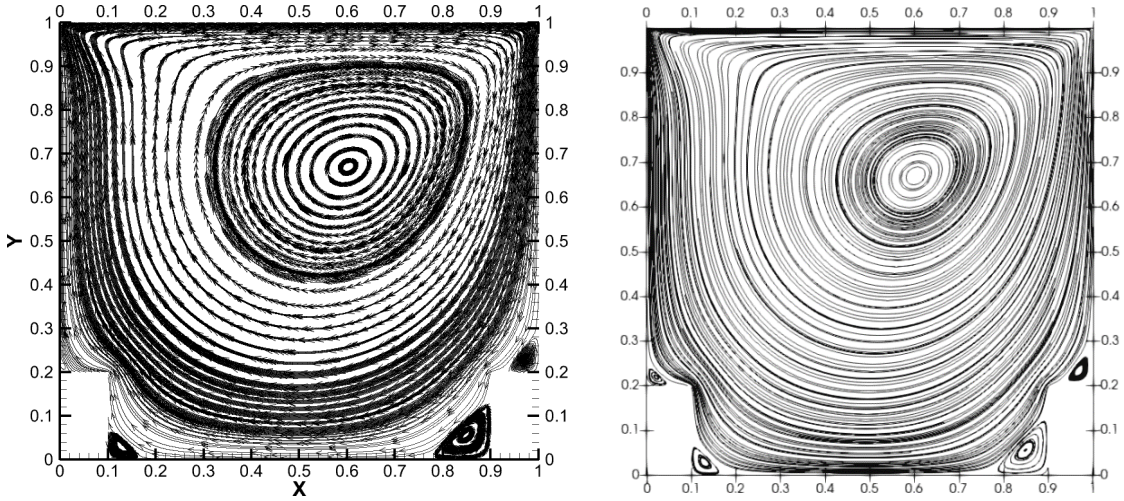

(a) $\mathrm{Re} = 200$

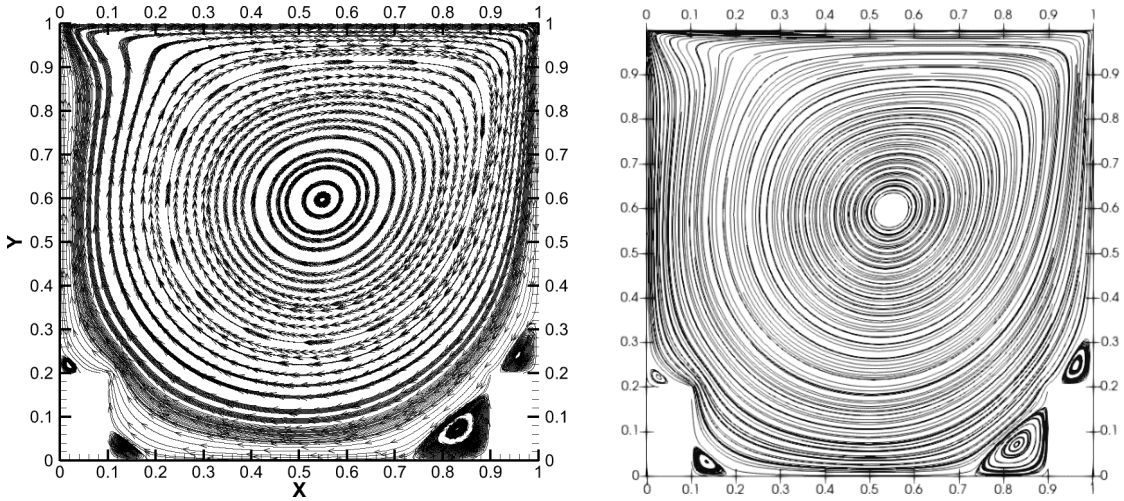

(b) $\mathrm{Re} = 500$

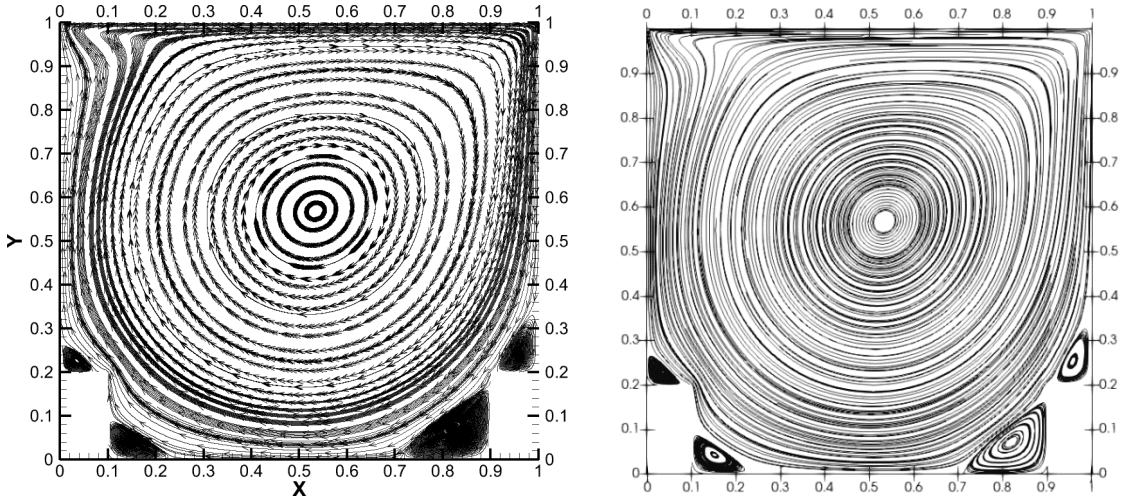

(c) $\mathrm{Re} = 1\,000$

Fig. 6. Streamline patterns in the single-sided T-shaped lid-driven cavity for different Reynolds numbers (AR $= 0.8$): (*left*) in-house code, (*right*) OpenFOAM

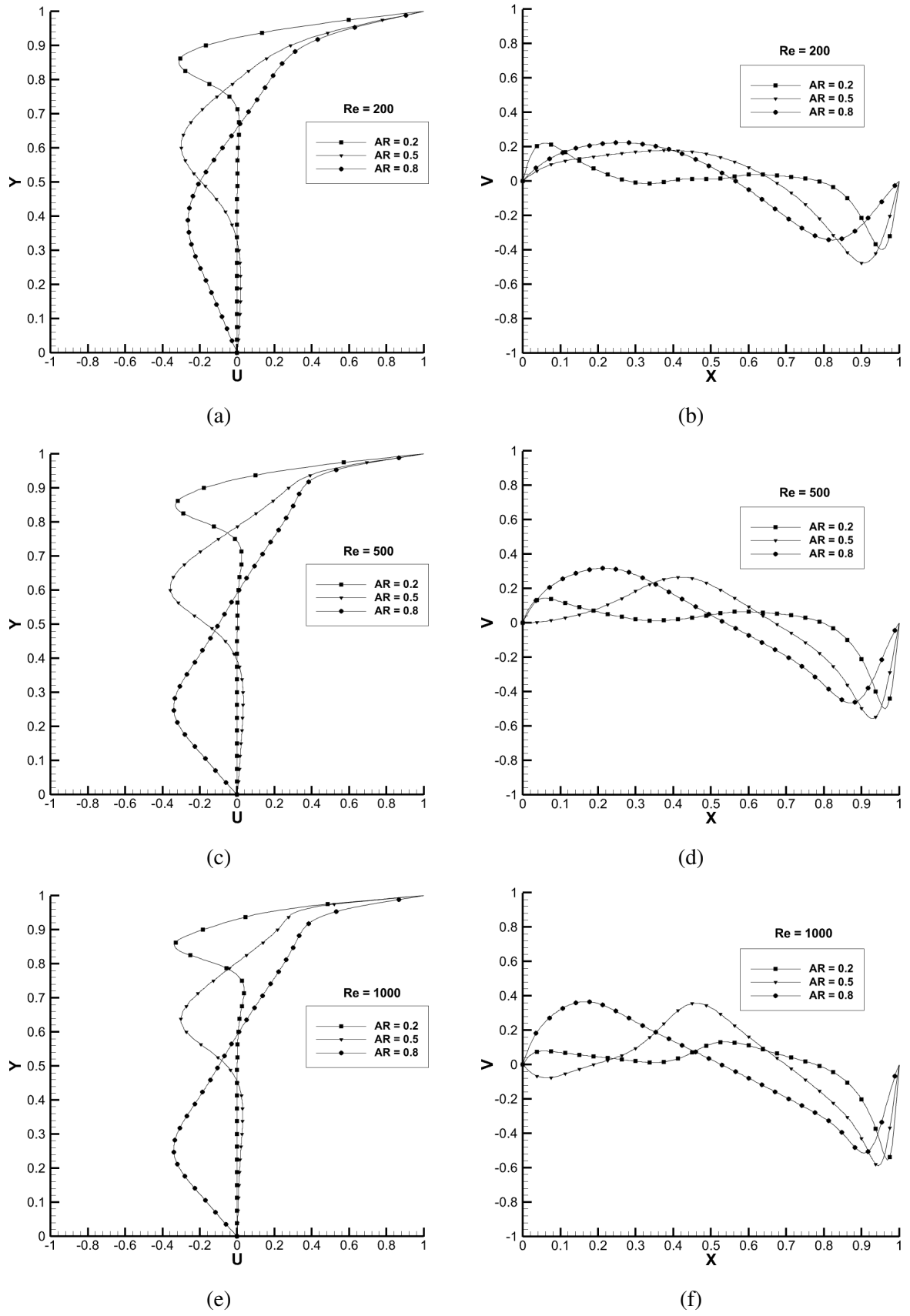

Fig. 7. Variations of u-velocity (*left*) and v-velocity (*right*) for single wall motion along the geometric centerline for different Reynolds numbers and aspect ratios

Table 4. Location of vortex cores in the single-sided T-shaped lid-driven square cavity for various aspect ratios at $\mathrm{Re} = 500$

Code	Aspect ratio	Primary vortex	Secondary vortex 1	Secondary vortex 2	Secondary vortex 3
In-house	0.2	(0.7952, 0.9072)	(0.5030, 0.7427)	(0.4995, 0.4623)	(0.5000, 0.1828)
OpenFOAM		(0.7853, 0.9175)	(0.5135, 0.7732)	(0.4879, 0.4548)	(0.5012, 0.1798)
In-house	0.5	(0.6687, 0.7719)	(0.4662, 0.3992)	(0.1490, 0.6027)	—
OpenFOAM		(0.6753, 0.7624)	(0.4712, 0.4002)	(0.1487, 0.5997)	—
In-house	0.8	(0.5483, 0.5973)	—	—	—
OpenFOAM		(0.5456, 0.5965)	—	—	—

This is a very desirable and well known characteristic, which leads to an increased intermixing of the fluid. The v-velocity plots of different aspect ratios have fairly distinct patterns for a given Reynolds number; this indicates that the aspect ratio plays a significant role in deciding the number of vortices formed at steady state and thereby enhances the mixing capabilities. However, the extrema of the velocities show variation due to the change in the aspect ratios. It would be quite fair to conclude from the velocity profiles that the cavity with an aspect ratio of 0.5 is the most effective at mixing liquids. Overall it can be concluded that a single lid-driven T-shaped cavity is suitable for carrying out an energy and mass transfer study inside the bounded domain. Table 4 presents the coordinates of the core of vortices in a single-sided T-shaped lid-driven square cavity for $\mathrm{Re} = 500$ for various aspect ratios. As the aspect ratio increases, the formation of secondary vortices disappears in the bounded domain.

3.2. Double-sided T-shaped lid-driven cavity with co-directional wall motion

With both top as well as bottom walls moving in co-directional motion, four recirculation zones are observed for $\mathrm{AR} = 0.2$ at all Reynolds numbers, Fig. 8. Although it is worth noting that the middle recirculation zone of the three recirculation zones in the narrow cavity keeps expanding with every Reynolds number increment and thereby pushes both the vortices adjoining it outward. At $\mathrm{AR} = 0.5$, the number of recirculation zones keeps increasing with subsequent Reynolds numbers from two to five, Fig. 9. The secondary vortices that develop at the corners of the cavities keep growing as the Reynolds number increases. It can be noted that just like in the case of the single lid-driven wall motion, the corner eddy tries to merge with the secondary vortex from the bottom due to the large step size of the cavity at $\mathrm{Re} = 1\,000$. However, at $\mathrm{AR} = 0.8$, much variation could not be observed except for an additional secondary vortex formed at $\mathrm{Re} = 500$ and $1\,000$, Fig. 10, and as anticipated, the secondary vortices keep increasing in size with an increase in the Reynolds number.

Fig. 11 shows centerline velocity variations for the different aspect ratios and Reynolds numbers considered in this study. Similarly to previous cases, it can be noted that the v-velocity

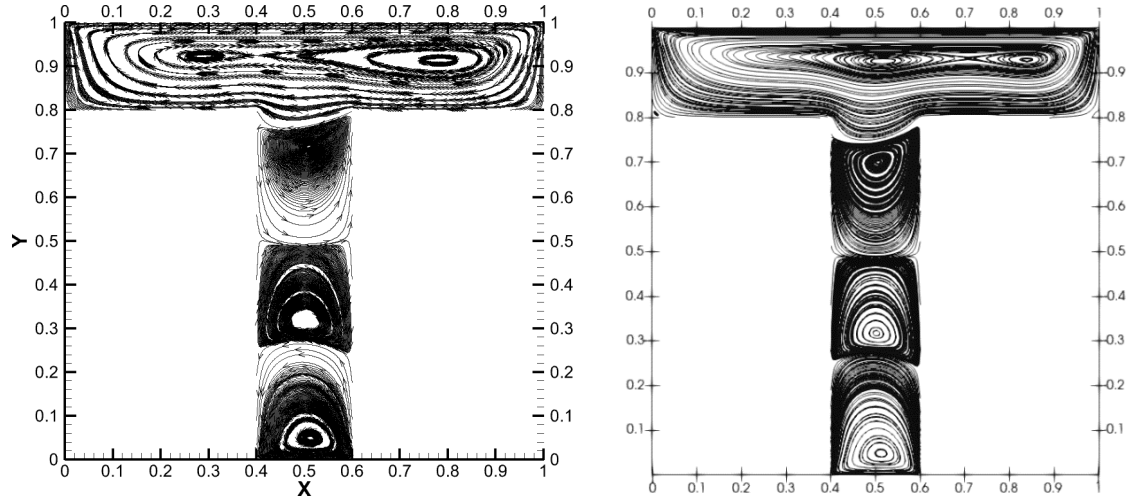

(a) Re = 200

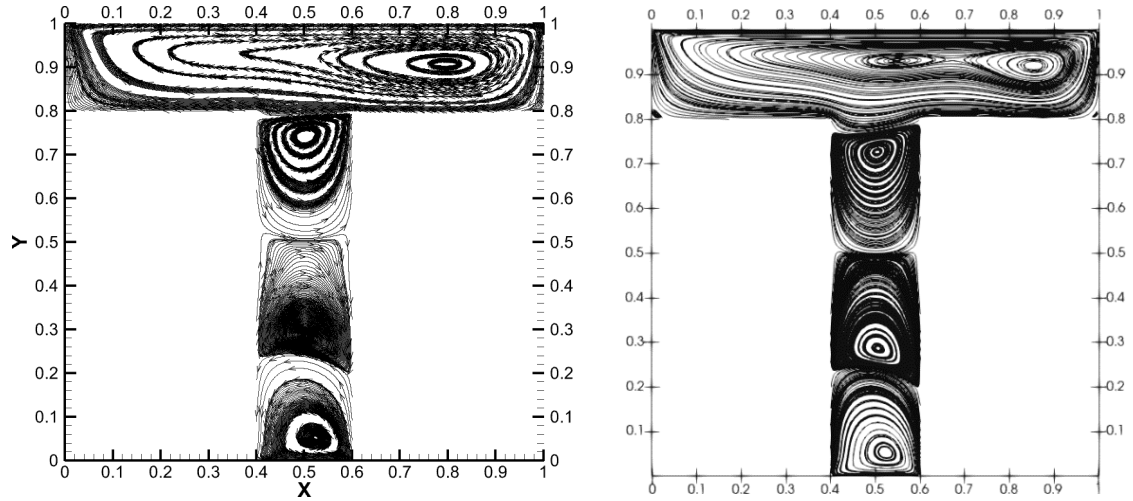

(b) Re = 500

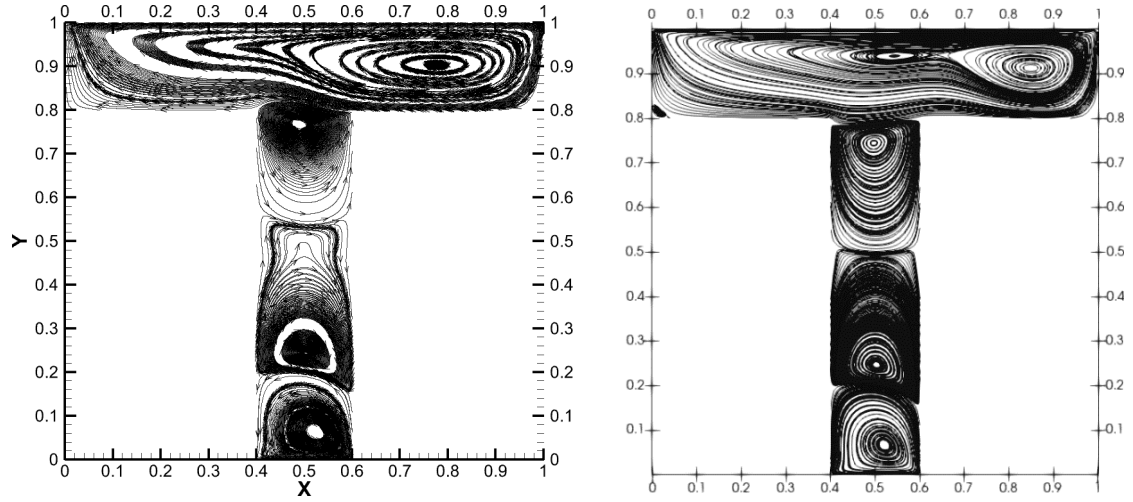

(c) Re = 1 000

Fig. 8. Streamline patterns in the double-sided T-shaped lid-driven cavity with co-directional motion for different Reynolds numbers (AR = 0.2): (*left*) in-house code, (*right*) OpenFOAM

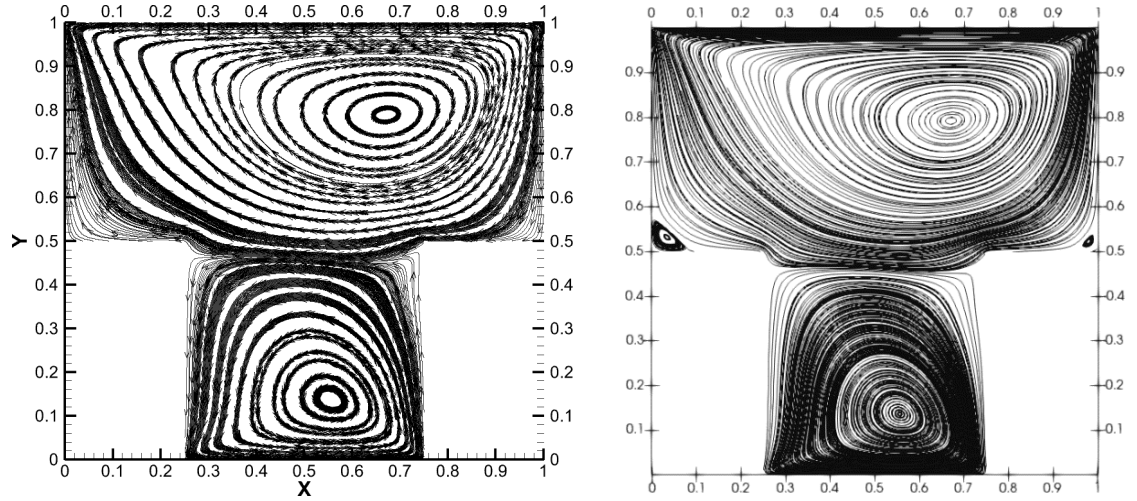

(a) $\mathrm{Re} = 200$

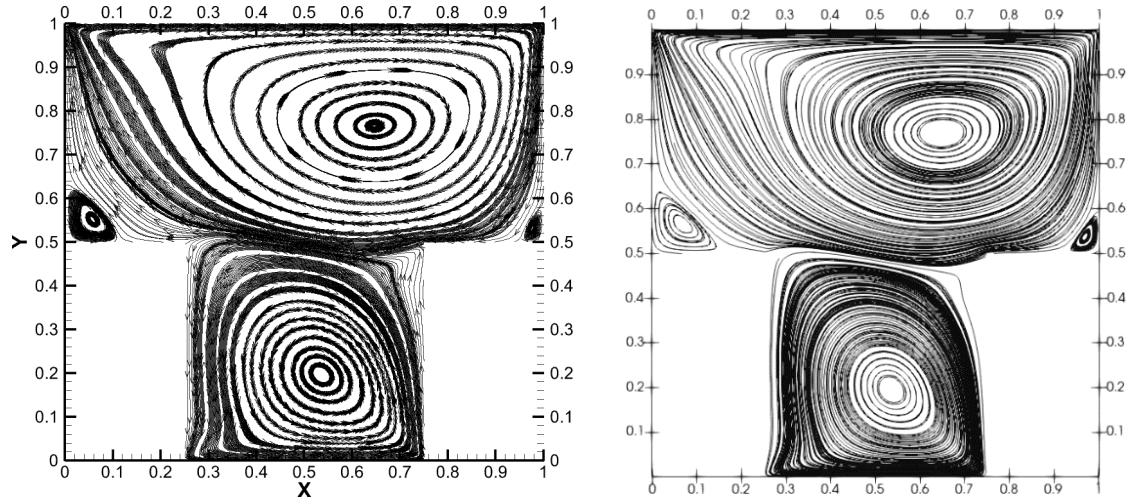

(b) $\mathrm{Re} = 500$

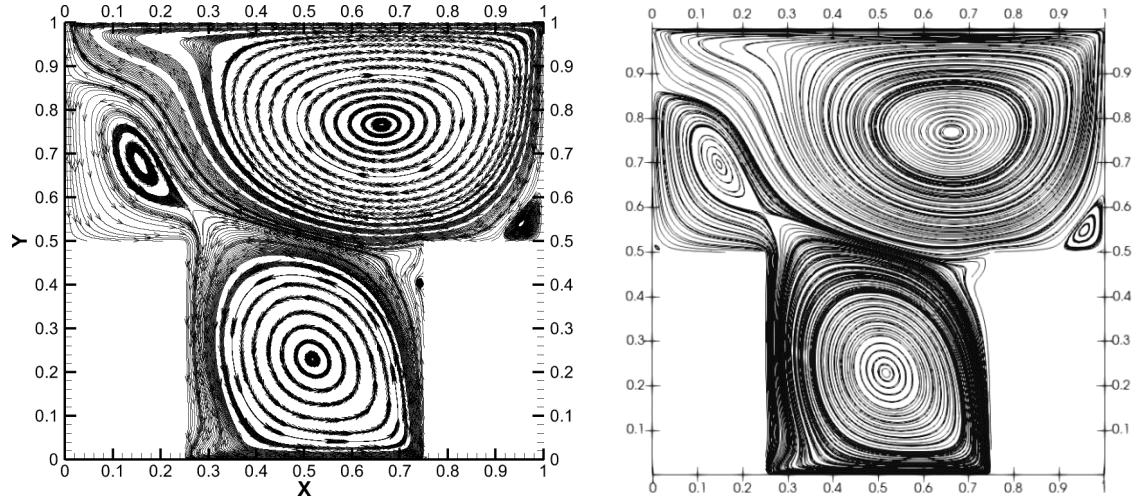

(c) $\mathrm{Re} = 1\,000$

Fig. 9. Streamline patterns in the double-sided T-shaped lid-driven cavity with co-directional motion for different Reynolds numbers (AR $= 0.5$): (*left*) in-house code, (*right*) OpenFOAM

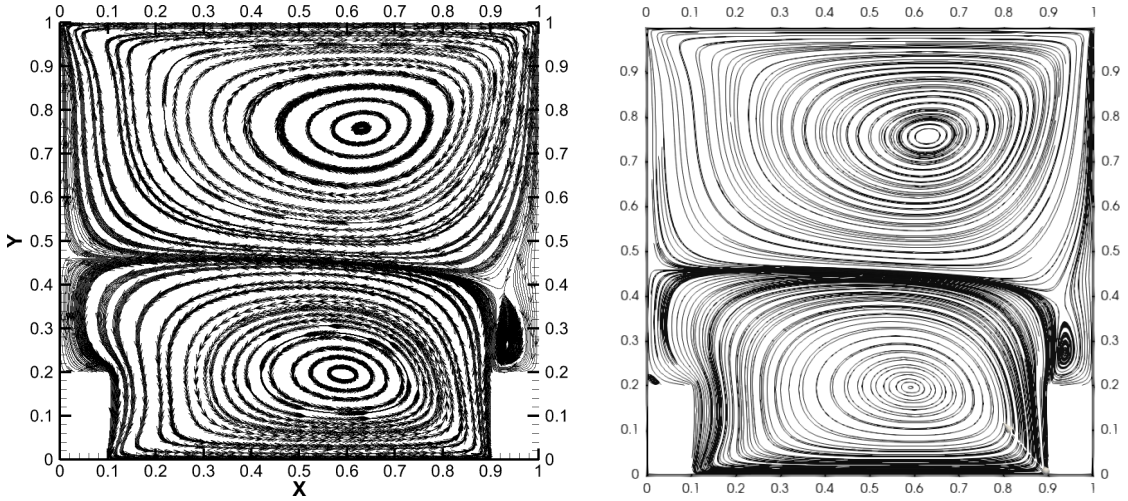

(a) $\mathrm{Re} = 200$

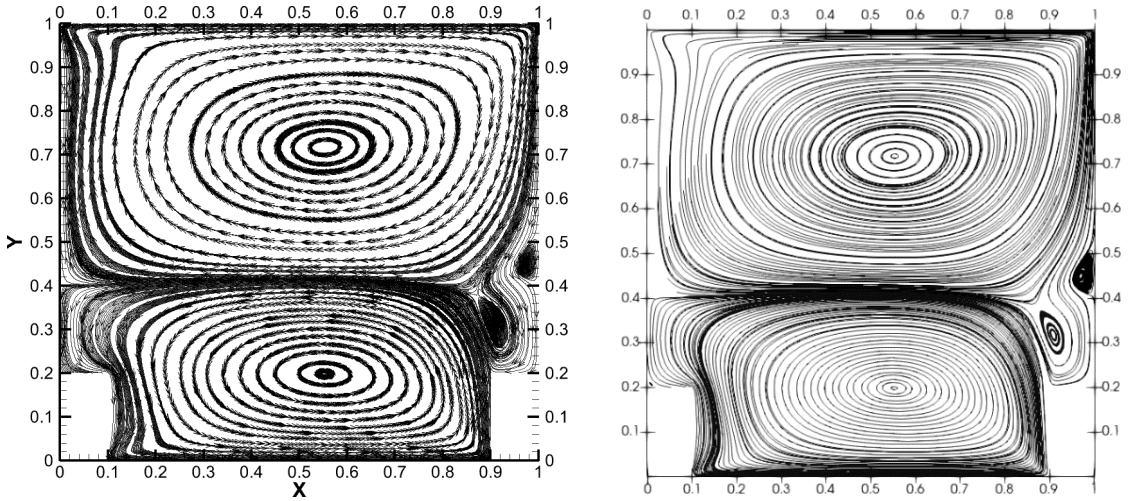

(b) $\mathrm{Re} = 500$

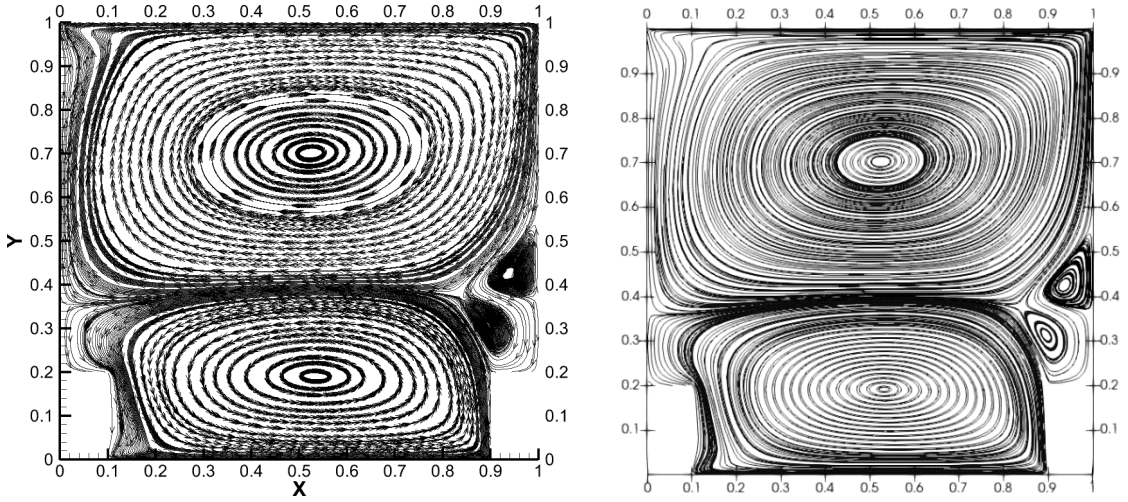

(c) $\mathrm{Re} = 1\,000$

Fig. 10. Streamline patterns in the double-sided T-shaped lid-driven cavity with co-directional motion for different Reynolds numbers (AR $= 0.8$): (*left*) in-house code, (*right*) OpenFOAM

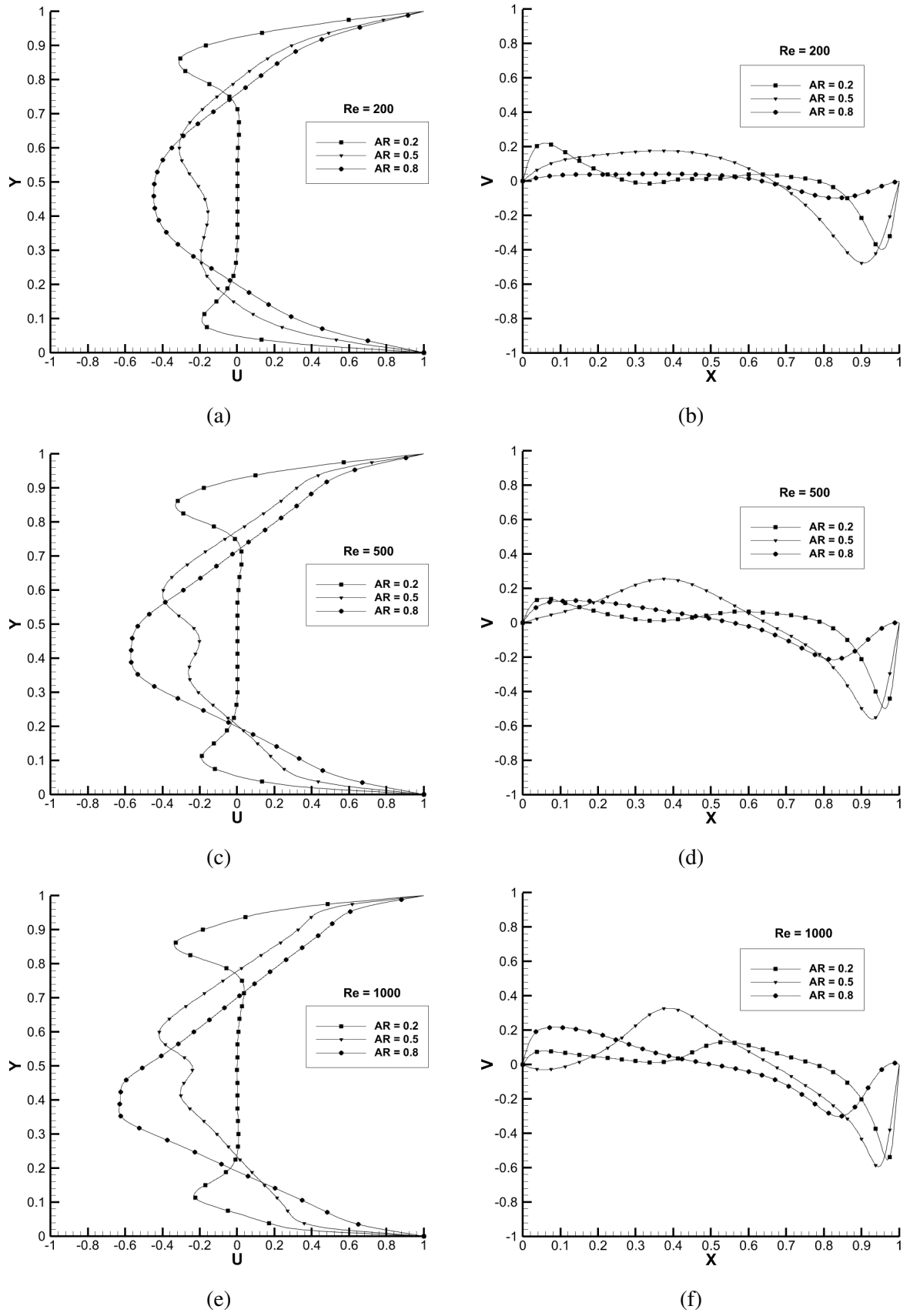

Fig. 11. Variations of u-velocity (*left*) and v-velocity (*right*) for co-directional wall motion along the geometric centerline for different Reynolds numbers and aspect ratios

Table 5. Location of vortex cores in the double-sided T-shaped lid-driven cavity with co-directional motion for various aspect ratios at $\mathrm{Re} = 500$

Code	Aspect ratio	Primary vortex	Secondary vortex 1	Secondary vortex 2	Secondary vortex 3
In-house	0.2	(0.7952, 0.9072)	(0.5030, 0.7427)	(0.5058, 0.2849)	(0.5240, 0.0524)
OpenFOAM		(0.7967, 0.9187)	(0.5068, 0.7419)	(0.5049, 0.2857)	(0.5342, 0.0556)
In-house	0.5	(0.6474, 0.7660)	(0.5356, 0.1962)	—	—
OpenFOAM		(0.6456, 0.7875)	(0.5328, 0.1978)	—	—
In-house	0.8	(0.5538, 0.7171)	(0.5530, 0.1980)	(0.9083, 0.3110)	—
OpenFOAM		(0.5576, 0.7186)	(0.5543, 0.1976)	(0.9074, 0.3145)	—

maxima are achieved for AR $= 0.5$ rather than 0.8 like in the single lid-driven motion. Apart from that, the mixing is noted to be enhanced from the previous case where the u-velocity profiles were analyzed. Based on the centerline velocity profiles, the aspect ratio of 0.5 outperforms other cavities in the case of co-directional wall configuration. Table 5 presents the coordinates of the vortex cores in the double-sided T-shaped lid-driven cavity with co-directional motion at $\mathrm{Re} = 200$ for various aspect ratios. It is apparent that as the aspect ratio increases, the primary vortex positions do not change much and secondary vortices disappear.

3.3. Double-sided T-shaped lid-driven cavity with counter-directional wall motion

For a counter-directional wall configuration, it is found that for AR $= 0.2$ the count of the vortices increases from four to five as the Reynolds number is increased from 200 to 500 and above, Fig. 12. The newly formed fifth recirculation zone forms as a result of both adjoining secondary vortices moving apart. As they keep moving apart with an increment in Reynolds number, the size of the newly formed secondary vortex keeps increasing. Streamline patterns of AR $= 0.5$ (Fig. 13) exhibit complex flow structures with two major recirculation zones and a minor eddy along the wall at $\mathrm{Re} = 200$. For an increased Reynolds number of 500, a total of five major recirculation zones are observed and also a Moffatt vortex is formed at the right corner. Three of the secondary vortices from $\mathrm{Re} = 500$ are seen coalescing at a Reynolds number of $1\,000$, thereby, forming three major recirculation zones with an enlarged Moffatt vortex from the previous case. Streamline patterns of AR $= 0.8$ (Fig. 14) do not change significantly. There is only one major recirculation zone, but an additional Moffatt vortex is induced for $\mathrm{Re} = 500$ and above. The recirculation area of the corner eddies increases with a subsequent increase in the Reynolds numbers.

The u-velocity centerline profiles that are presented in Fig. 15 indicate that extensive mixing takes place in the case with anti-co-directional motion in comparison with the rest. The v-velocity profiles are also a bit different from the previous cases and here it is seen that the aspect ratio of 0.8 has the largest extreme value compared to the other Reynolds numbers. The

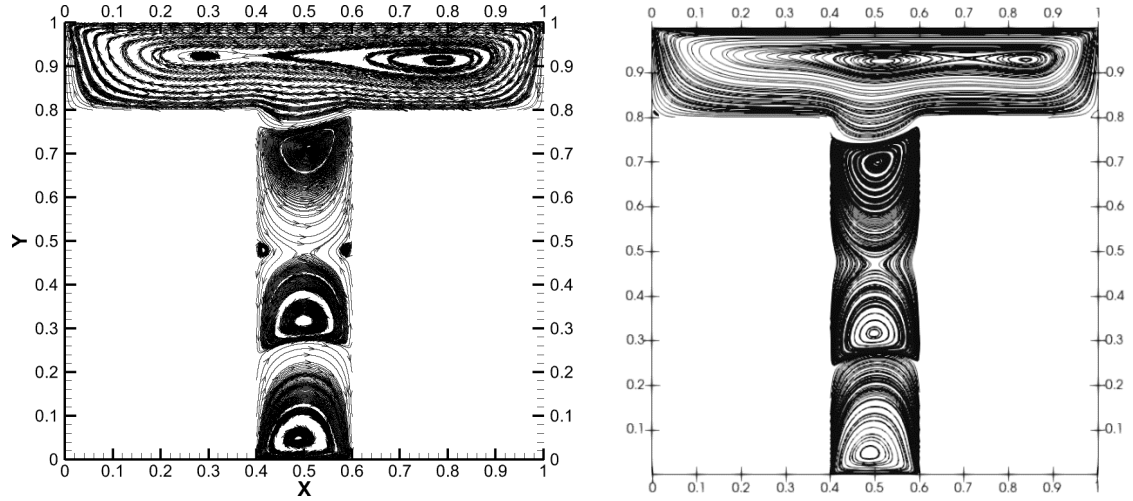

(a) $\mathrm{Re} = 200$

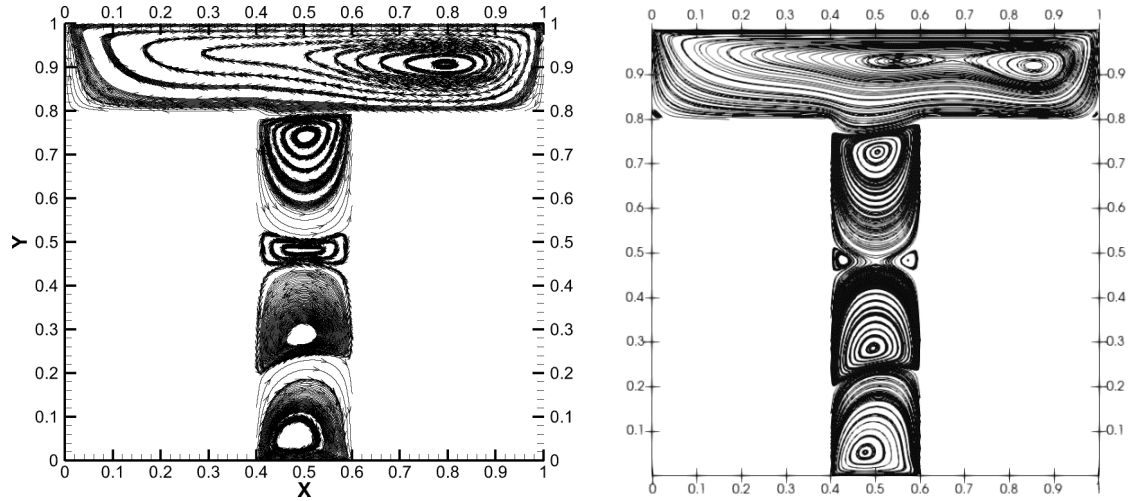

(b) $\mathrm{Re} = 500$

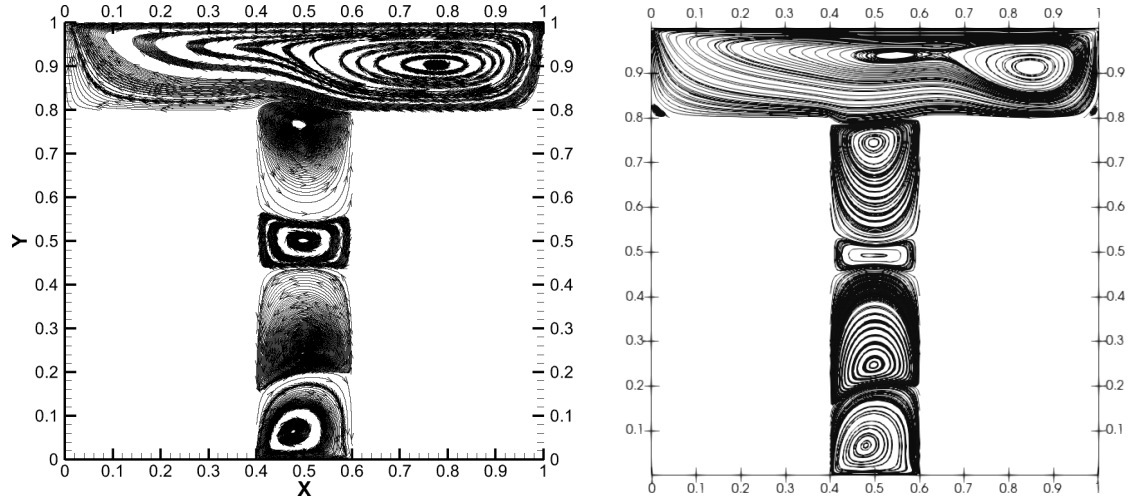

(c) $\mathrm{Re} = 1\,000$

Fig. 12. Streamline patterns in the double-sided T-shaped lid-driven cavity with counter-directional motion for different Reynolds numbers (AR $= 0.2$): (*left*) in-house code, (*right*) OpenFOAM

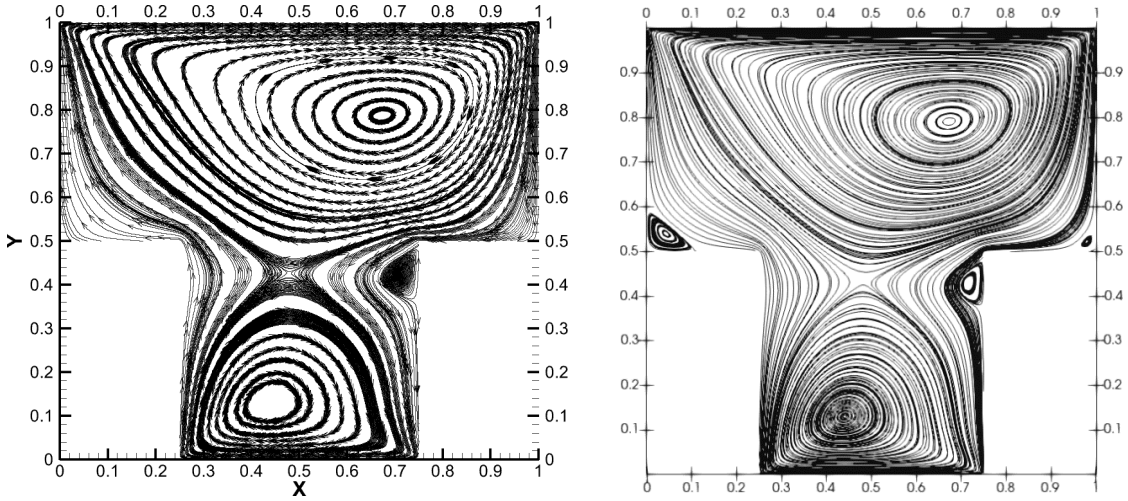

(a) Re = 200

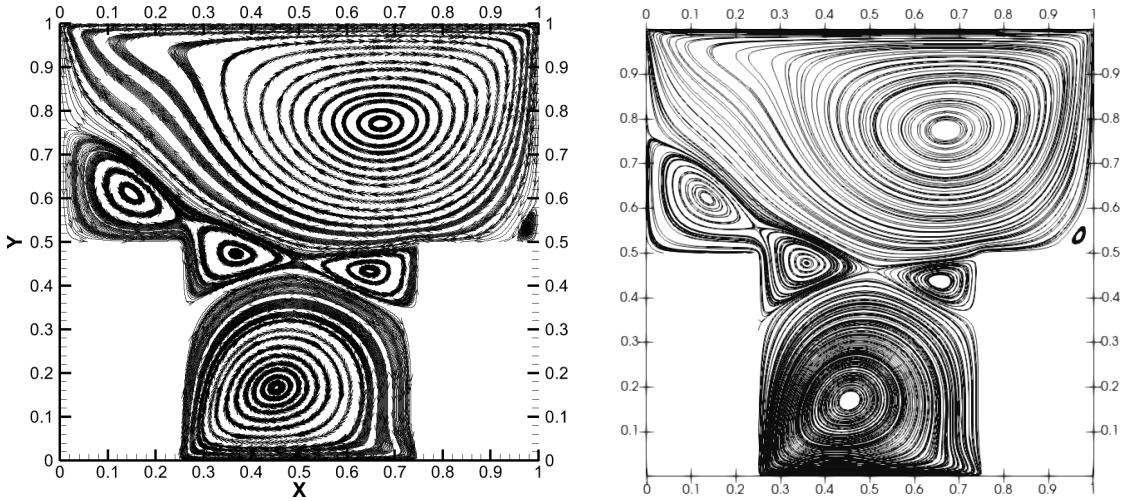

(b) Re = 500

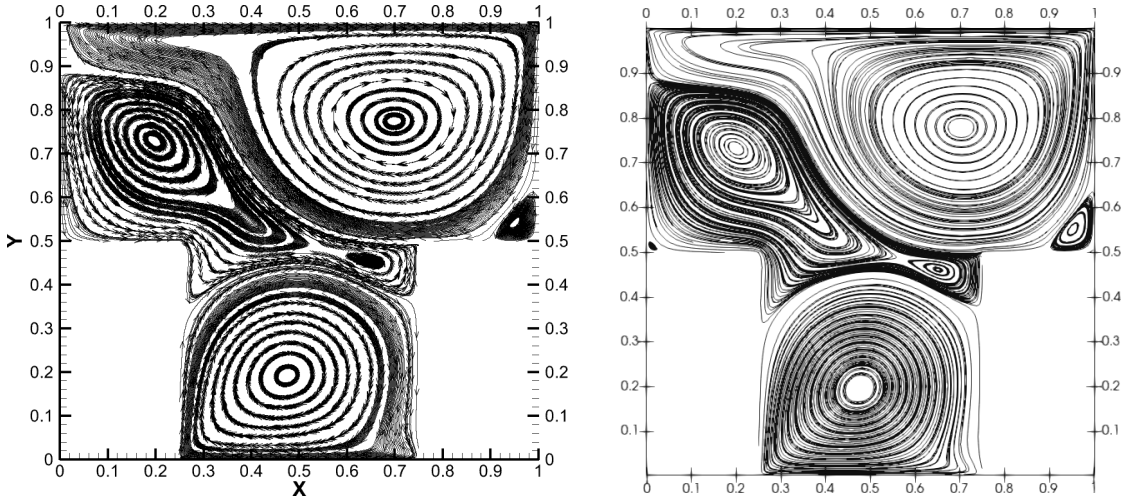

(c) Re = 1 000

Fig. 13. Streamline patterns in the double-sided T-shaped lid-driven cavity with counter-directional motion for different Reynolds numbers (AR = 0.5): (*left*) in-house code, (*right*) OpenFOAM

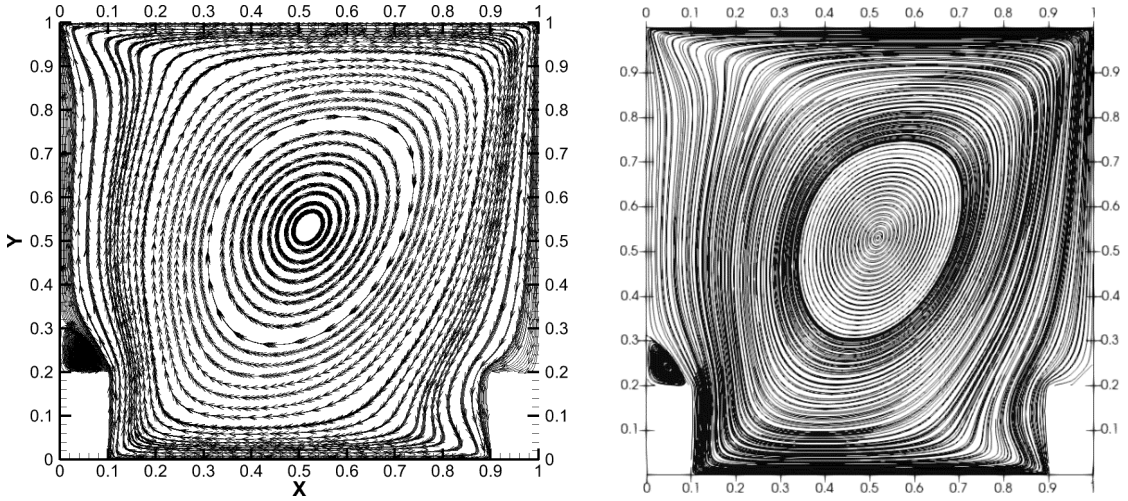

(a) $\mathrm{Re} = 200$

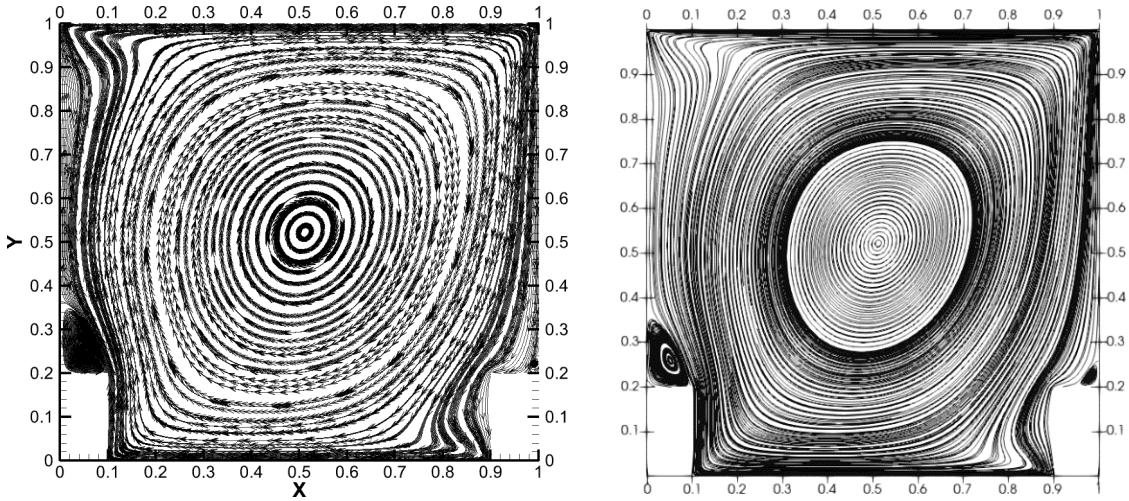

(b) $\mathrm{Re} = 500$

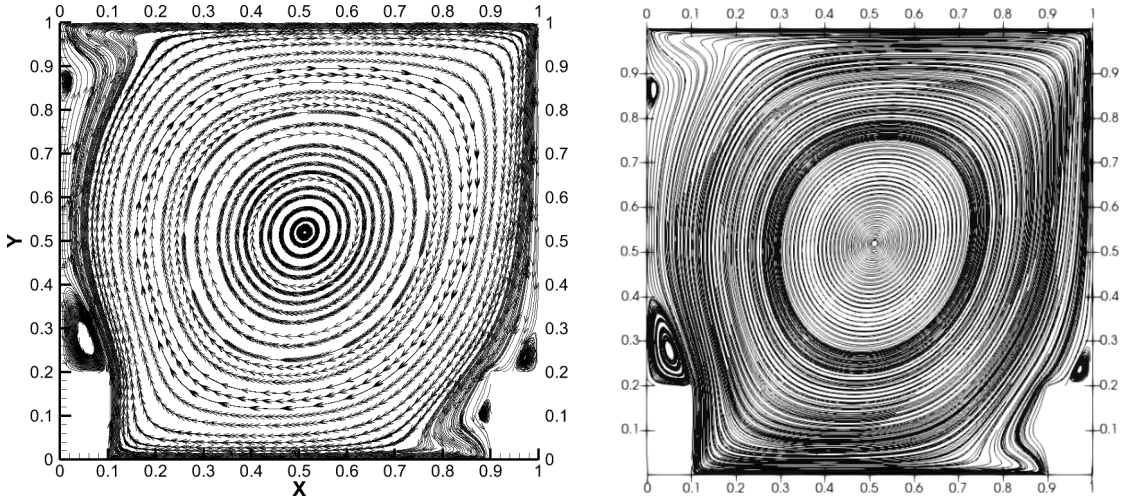

(c) $\mathrm{Re} = 1\,000$

Fig. 14. Streamline patterns in the double-sided T-shaped lid-driven cavity with counter-directional motion for different Reynolds numbers (AR $= 0.8$): (*left*) in-house code, (*right*) OpenFOAM

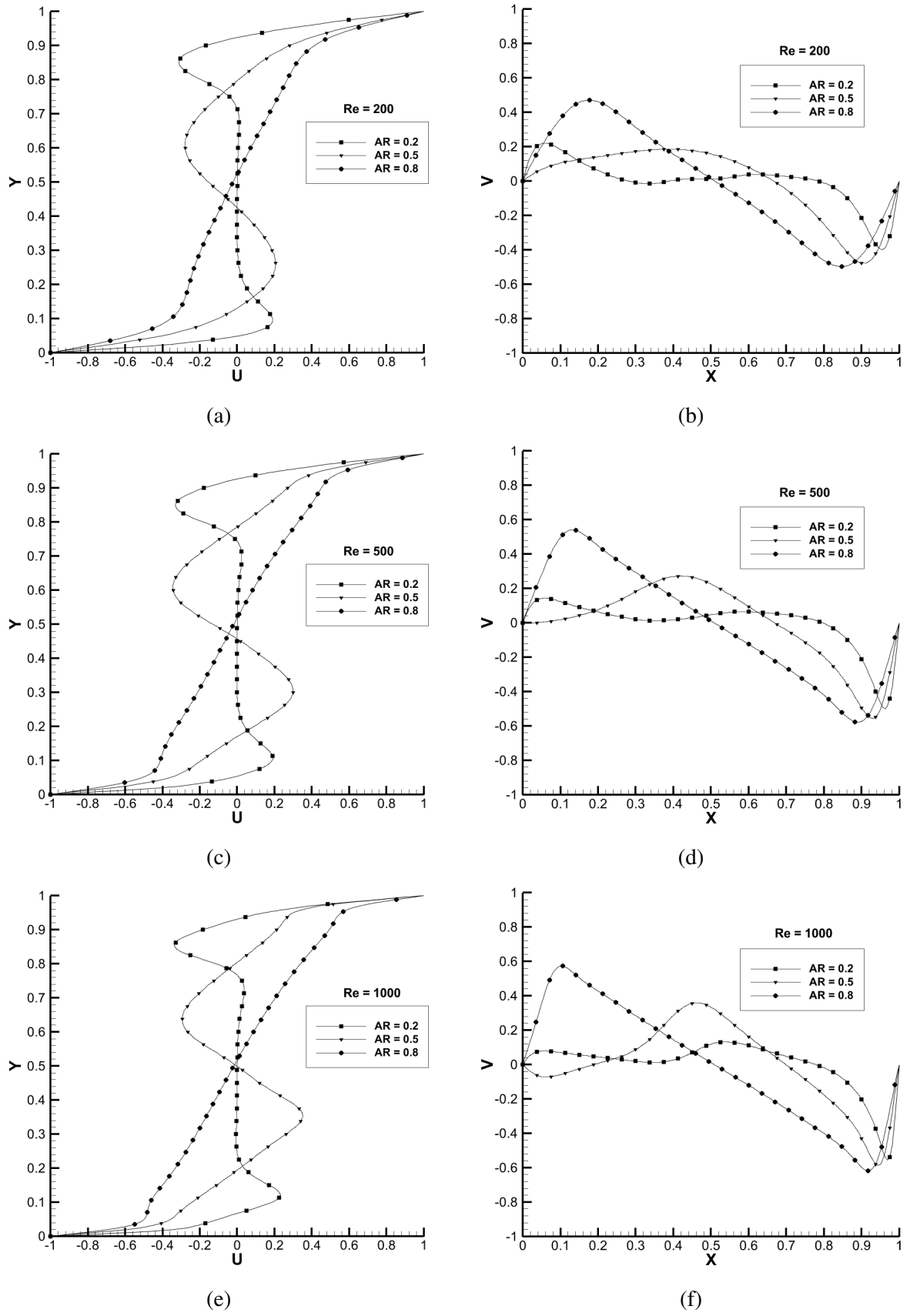

Fig. 15. Variations of u-velocity (*left*) and v-velocity (*right*) for counter-directional wall motion along the geometric centerline for different Reynolds numbers and aspect ratios

Table 6. Location of vortex cores in the double-sided T-shaped lid-driven cavity with counter-directional motion for various aspect ratios at $\mathrm{Re} = 500$

Code	Aspect ratio	Primary vortex	Secondary vortex 1	Secondary vortex 2	Secondary vortex 3
In-house	0.2	(0.7952, 0.9072)	(0.5030, 0.7427)	(0.4940, 0.2847)	(0.4759, 0.0524)
OpenFOAM		(0.7968, 0.9083)	(0.5124, 0.7437)	(0.4936, 0.2876)	(0.4762, 0.0554)
In-house	0.5	(0.6692, 0.7710)	(0.4523, 0.1666)	(0.1484, 0.1666)	—
OpenFOAM		(0.6754, 0.7765)	(0.4543, 0.1672)	(0.1492, 0.1676)	—
In-house	0.8	(0.5117, 0.5222)	—	—	—
OpenFOAM		(0.5121, 0.5233)	—	—	—

values of the v-velocity change from quite large negative values to positive values throughout the horizontal length of the cavity. The trends of the centerline velocity profiles for all wall motions are similar to that of Perumal and Dass [22] and Bhopalam and Perumal [2] who also simulated all three wall motions for a square cavity and a L-shaped cavity, respectively. Table 6 lists the coordinates of the vortex cores in the double-sided T-shaped lid-driven cavity with counter-directional motion at $\mathrm{Re} = 200$ for various aspect ratios. It is apparent that the position of vortices follows a similar trend of the other directional motions.

Here, OpenFOAM produced quite reasonable results on the 10^5 mesh with near-wall grid spacing. The results for the shear-flow at various Reynolds numbers of 200, 500, and 1000 did not significantly improve when the mesh size was increased from 10^5 to $5 \cdot 10^5$. Therefore, it does not seem that there are any resolution-related reasons for the discrepancies between OpenFOAM and the in-house code. They may have something to do with the second-order spatial discretization schemes, which are comparatively lower. Since structured quadrilateral (2D) meshes were employed in this work, more complicated geometries with a variety of cell types are advised as this could have an impact on the accuracy of the OpenFOAM results.

OpenFOAM and the in-house code are compared for counter-directional, co-directional and single wall motion for $\mathrm{Re} = 1\,000$ and AR $= 0.8$ in Figs. 16, 17 and 18, respectively. It is found that the results from the in-house code and OpenFOAM are in close agreement with each other. The solvers in OpenFOAM are well generalized for this flow condition such that the in-house code data (Fig. 7e–f) are in agreement with the OpenFOAM output. This further clarifies the general motion setup in T-shaped junction with parallel (Fig. 11e–f) and anti-parallel motion (Fig. 15e–f). The in-house code can be formalized to work in extended flow environments to establish the standards of the OpenFOAM solver in the form of streamlines, centerline velocity plots and location of stagnation points. All of the present computations were carried out on a Pentium-based PC with 1 GB RAM.

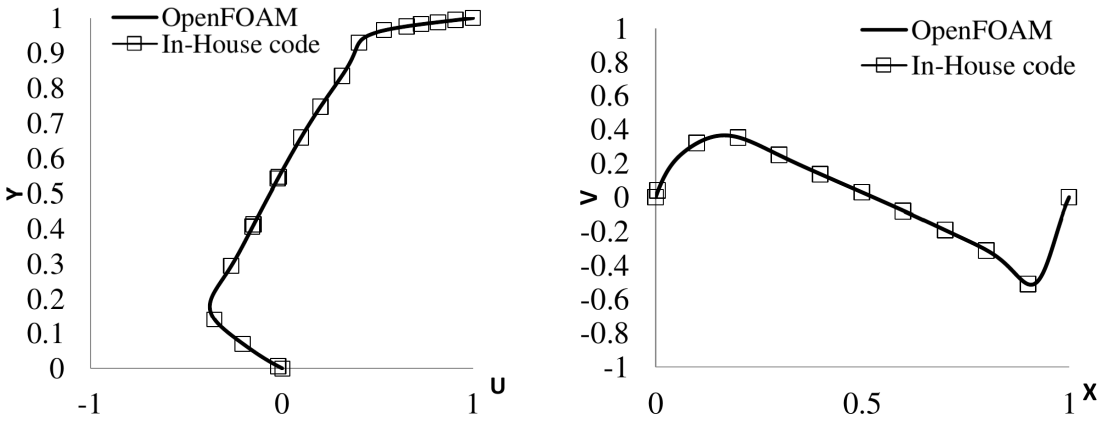

(a) (b)

Fig. 16. Comparison of OpenFOAM and in-house code for AR $= 0.8$ and $\mathrm{Re} = 1\,000$ in single wall motion along the geometric centerline

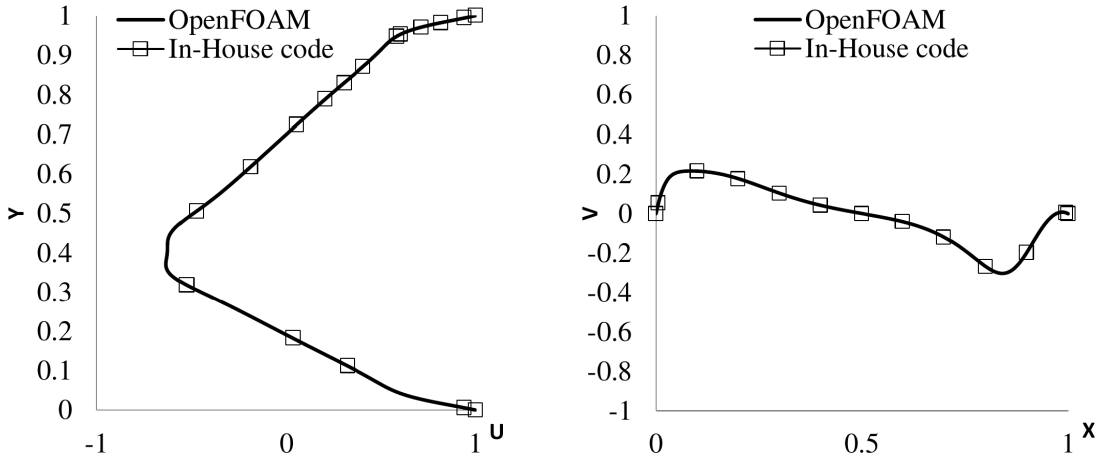

(a) (b)

Fig. 17. Comparison of OpenFOAM and in-house code for AR $= 0.8$ and $\mathrm{Re} = 1\,000$ in co-directional wall motion along the geometric centerline

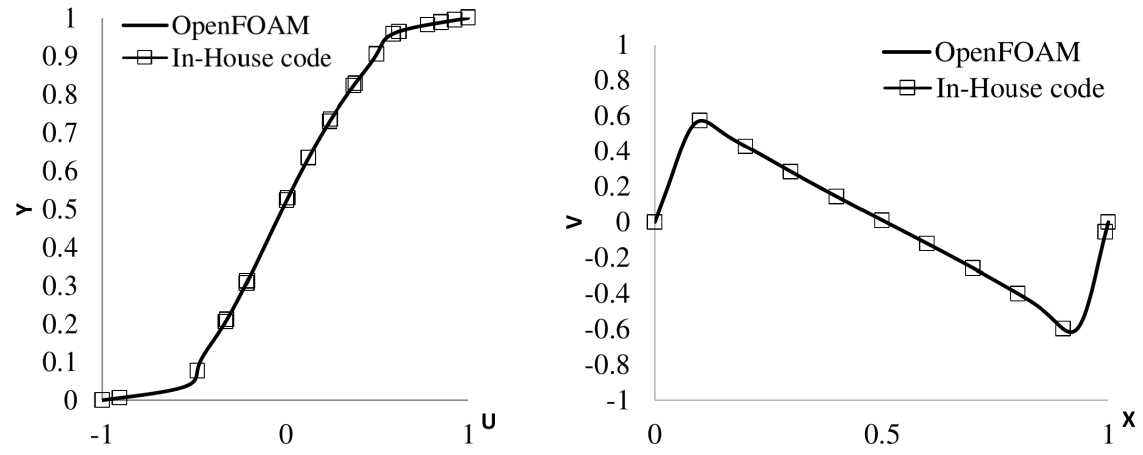

(a) (b)

Fig. 18. Comparison of OpenFOAM and in-house code for AR $= 0.8$ and $\mathrm{Re} = 1\,000$ in counter-directional wall motion along the geometric centerline

4. Conclusions

The flow phenomena in a T-shaped cavity was analyzed using a FDM in-house code as well as the OpenFOAM solver. The well-known continuity and momentum equations for laminar incompressible flow were solved in order to determine the flow in the T-shaped cavity of the constructed model, treating the pressure in semi-implicit form. The flow patterns in the T-shaped cavity have been analyzed for different aspect ratios and Reynolds numbers. From the streamline patterns and the velocity variation along the centerline, it can be concluded that the T-shaped cavity proves to be exceptional for fluid mixing processes as various recirculation zones are induced in the cavity. It seems to be a better alternative than a square cavity for energy and mass transfer purposes. Both the FDM-based in-house code and FVM-based OpenFOAM (SimpleFoam solver) are in close agreement in the streamline patterns, velocity profiles and position of vortices. It can be concluded that as the Reynolds number is increased, the recirculation zones increase in size and the extrema of the centerline velocity profiles increase, enhancing mixing performance.

- In conclusion, with an increase in the flow's Reynolds number, it is observed that the area of recirculation zones increases as well as the extrema of the centerline velocity profiles rises, enhancing mixing performance.
- The aspect ratio has a very significant effect on the flow in terms of streamline patterns, and it can be seen to affect the number of formed corner eddies and can also provide the facility for some of these corner eddies to increase in size with a subsequent increase in the Reynolds number. It is also the most influential factor in deciding the number of primary recirculation zones at steady state.
- Wall motions and direction of flows have an important effect on the centerline velocity profiles, thereby playing a major role in enhancing the mixing performance, with counter-directional motion being the most suitable for improving mixing.
- The T-shaped cavity, due to its narrow cavity width for particular aspect ratios, behaves like a deep cavity (also known as a L-shaped cavity), in terms of the number of formed recirculation zones and overall flow characteristics.
- Both the in-house code and the OpenFOAM solver can solve the problem to a similar accuracy.

References

[1] Ahmed, M., Kuhlmann, H. C., Flow instability in triangular lid-driven cavities with wall motion away from a rectangular corner, Fluid Dynamics Research 44 (2) (2012) No. 025501. https://doi.org/10.1088/0169-5983/44/2/025501

[2] Bhopalam, S. R., Perumal, D. A., Numerical analysis of fluid flows in L-shaped cavities using lattice Boltzmann method, Applications in Engineering Science 3 (2020) No. 100016. https://doi.org/10.1016/j.apples.2020.100016

[3] Bhopalam, S. R., Perumal, D. A., Yadav, A. K., Computation of fluid flow in double sided cross-shaped lid driven cavities using lattice Boltzmann method, European Journal of Mechanics – Part B/Fluids 70 (2018) 46–72. https://doi.org/10.1016/j.euromechflu.2018.01.006

[4] Bisht, M., Haeri, S., Patil, D. V., Fluid flow in wall-driven enclosures with corrugated bottom, Computers & Fluids 152 (2017) 1–13. https://doi.org/10.1016/j.compfluid.2017.04.008

[5] Burggraf O. R., Analytical and numerical studies of the structure of steady separated flows, Journal of Fluid Mechanics 24 (1) (1966) 113–151. https://doi.org/10.1017/S0022112066000545

[6] Erturk, E., Gokcol, O., Fine grid numerical solutions of triangular cavity flow, The European Physical Journal – Applied Physics 38 (1) (2007) 97–105. https://doi.org/10.1051/epjap:2007057

[7] Fatima, N., Rajan, I., Perumal, D. A., Sasithradevi, A., Ahmed, S. A. A., Gorji, M. R., Ahmad, Z., Simulation of fluid flow in a lid-driven cavity with different wave lengths corrugated walls using lattice Boltzmann method, Journal of the Taiwan Institute of Chemical Engineers 144 (2023) No. 104748. https://doi.org/10.1016/j.jtice.2023.104748

[8] Ghia, U., Ghia, K. N., Shin, C. T., High-Re solutions for incompressible flow using the Navier–Stokes equations and a multigrid method, Journal of Computational Physics 48 (3) (1982) 387–411. https://doi.org/10.1016/0021-9991(82)90058-4

[9] Goodrich, J. W., Gustafson, K., Halasi, K., Hopf bifurcation in the driven cavity, Journal of Computational Physics 90 (1) (1990) 219–261. https://doi.org/10.1016/0021-9991(90)90204-E

[10] Jagannathan, A., Mohan, R., Dhanak, M., A spectral method for the triangular cavity flow, Computers & Fluids 95 (2014) 40–48. https://doi.org/10.1016/j.compfluid.2014.02.003

[11] Kelmanson, M. A., Lonsdale, B., Eddy genesis in the double-lid-driven cavity, The Quarterly Journal of Mechanics and Applied Mathematics 49 (4) (1996) 635–655. https://doi.org/10.1093/qjmam/49.4.635

[12] Kuhlmann, H. C., Wanschura, M., Rath, H. J., Elliptic instability in two-sided lid-driven cavity flow, European Journal of Mechanics – Part B/Fluids 17 (4) (1998) 561–569. https://doi.org/10.1016/S0997-7546(98)80011-3

[13] Kuhlmann, H. C., Wanschura, M., Rath, H. J., Flow in two-sided lid-driven cavities: Non-uniqueness, instabilities, and cellular structures, Journal of Fluid Mechanics 336 (1997) 267–299. https://doi.org/10.1017/S0022112096004727

[14] McQuain, W. D., Ribbens, C. J., Wang, C.-Y., Watson, L. T., Steady viscous flow in a trapezoidal cavity, Computers & Fluids 23 (4) (1994) 613–626. https://doi.org/10.1016/0045-7930(94)90055-8

[15] Moffatt, H. K., Viscous and resistive eddies near a sharp corner, Journal of Fluid Mechanics 18 (1) (1964) 1–18. https://doi.org/10.1017/S0022112064000015

[16] Naeem, A. B., A numerical and experimental study of lid driven square cavity flow for laminar and turbulent cases, Master thesis, University of New Orleans, New Orleans, 2020.

[17] Pan, F., Acrivos, A., Steady flows in rectangular cavities, Journal of Fluid Mechanics 28 (4) (1967) 643–655. https://doi.org/10.1017/S002211206700237X

[18] Park, S., Direct numerical simulation for lid driven cavity under various Reynolds number in fully staggered grid, Physics of Fluids 35 (11) (2023) No. 115110. https://doi.org/10.1063/5.0169418

[19] Patil, D. V., Lakshmisha, K. N., Rogg, B., Lattice Boltzmann simulation of lid-driven flow in deep cavities, Computers & Fluids 35 (10) (2006) 1 116–1 125. https://doi.org/10.1016/j.compfluid.2005.06.006

[20] Perng, C. Y., Street, R. L., A coupled multigrid-domain splitting technique for simulating incompressible flows in geometrically complex domains, International Journal of Numerical Methods in Fluids 13 (3) (1991) 269–286. https://doi.org/10.1002/fld.1650130302

[21] Perumal, D. A., Dass, A. K., Application of lattice Boltzmann method for incompressible viscous flows, Applied Mathematical Modelling 37 (6) (2013) 4 075–4 092. https://doi.org/10.1016/j.apm.2012.09.028

[22] Perumal, D. A., Dass, A. K., Simulation of incompressible flows in two-sided lid–driven square cavities. Part I – FDM, CFD Letters 2 (1) (2010) 13–24.

[23] Rajan I., Perumal, D. A., Flow dynamics of lid-driven cavities with obstacles of various shapes and configurations using the lattice Boltzmann method, Journal of Thermal Engineering 7 (2) (2021) 83–102. https://doi.org/10.18186/thermal.869135

[24] Shankar, P. N., Deshpande, M. D., Fluid mechanics in the driven cavity, Annual Review of Fluid Mechanics 32 (2000) 93–136. https://doi.org/10.1146/annurev.fluid.32.1.93

[25] Shen, J., Hopf bifurcation of the unsteady regularized driven cavity flow, Journal of Computational Physics 95 (1) (1991) 228–245. https://doi.org/10.1016/0021-9991(91)90261-I

[26] Shetty, V. V, Balashanker, K., Perumal, D. A., Patel, V. U., Analysis of fluid flows in bounded domain with particular shape of a cavity using lattice Boltzmann method, Recent Patents on Mechanical Engineering 16 (5) (2023) 359–372.
https://doi.org/10.2174/2212797616666230803115517

[27] Zhang, T., Shi, B., Chai, Z., Lattice Boltzmann simulation of lid-driven flow in trapezoidal cavities, Computers & Fluids 39 (10) (2010) 1 977–1 989.
https://doi.org/10.1016/j.compfluid.2010.06.027